
BAYESIAN CONDITIONAL AUTO-REGRESSIVE LASSO MODELS TO LEARN SPARSE BIOLOGICAL NETWORKS WITH PREDICTORS

Yunyi Shen

Department of Statistics
University of Wisconsin-Madison
Madison, WI 53706

Claudia Solís-Lemus*

Wisconsin Institute for Discovery
University of Wisconsin-Madison
Madison, WI 53706

ABSTRACT

Microbiome data analyses require statistical models that can simultaneously decode microbes' reaction to the environment and interactions among microbes. While a multiresponse linear regression model seems like a straight-forward solution, we argue that treating it as a graphical model is flawed given that the regression coefficient matrix does not encode the conditional dependence structure between response and predictor nodes because it does not represent the adjacency matrix. This observation is especially important in biological settings when we have prior knowledge on the edges from specific experimental interventions that can only be properly encoded under a conditional dependence model. Here, we propose a chain graph model with two sets of nodes (predictors and responses) whose solution yields a graph with edges that indeed represent conditional dependence and thus, agrees with the experimenter's intuition on the average behavior of nodes under treatment. The solution to our model is sparse via Bayesian LASSO and is also guaranteed to be the sparse solution to a Conditional Auto-Regressive (CAR) model. In addition, we propose an adaptive extension so that different shrinkage can be applied to different edges to incorporate edge-specific prior knowledge. Our model is computationally inexpensive through an efficient Gibbs sampling algorithm and can account for binary, counting and compositional responses via appropriate hierarchical structure. We apply our model to a human gut and a soil microbial compositional datasets and we highlight that CAR-LASSO can estimate biologically meaningful network structures in the data. The CAR-LASSO software is available as an R package at <https://github.com/YunyiShen/CAR-LASSO>.

Keywords Linear Regression · Compositional Data · Interaction Network · Chain graph

1 Introduction

Recent years have seen explosion of microbiome research studies given that microbial communities are among the main driving forces of all biogeochemical processes on Earth. On one side, many critical soil processes such as mineral weathering, and soil cycling of mineral-sorbed organic matter are governed by mineral-associated microbes (Fierer et al., 2012; Whitman et al., 2018; Cates et al., 2019; Kranz and Whitman, 2019; Whitman et al., 2019). On another side, plant and soil microbiome drive phenotype variation related to plant health and crop production (Allsup and Lankau, 2019; Rioux et al., 2019; Lankau et al., 2020b,a). In addition, as evidenced by The Human Microbiome Project (Turnbaugh et al., 2007), the microbes that live on the human body are key determinants of human health and disease (Dave et al., 2012).

Understanding the composition of microbial communities and what environmental or experimental factors play a role in shaping this composition is crucial to comprehend biological processes in humans, soil and plants alike, and to predict microbial responses to environmental changes. However, the inter-connectivity of microbes-environment is still not fully understood. One of the reasons for this gap in knowledge is the lack of statistical tools to infer connections among microbial communities while simultaneously accounting for predictors in an unified framework.

On the surface, the solution to this problem in linear regression settings seems straight-forward. On one side, a multiresponse linear regression model in conjunction with LASSO techniques allows us to estimate sparse links between multiple responses and predictors and this setup could potentially be treated as a graphical model. On the other side, (bayesian) graphical LASSO (Friedman et al., 2008; Wang, 2012) allows us to determine a sparse graphical model

*Corresponding author: solislemus@wisc.edu

representation among responses via estimation of the sparse covariance matrix albeit without the inclusion of predictors. Intuitively, the combination of these methods would provide a framework where researchers could estimate a sparse graphical structure with nodes for responses and for predictors.

We argue, however, that treating a multiresponse linear regression model as a graphical model is flawed and it should be done with caution. In particular, care should be taken to distinguish between marginal effects and conditional effects. This distinction is crucial when we would like to include biological prior knowledge to the model (e.g. as in [Lo and Marculescu \(2017\)](#)). For instance, penicillin has no biological effect on Gram-negative bacteria, yet it might still promote the abundance of such bacteria by inhibiting their Gram-positive competitors. In this example, penicillin has no *conditional* effect on Gram-negative nodes (conditioned on all other microbes), but it may have a *marginal* effect on them when marginalizing over all other microbes (Figure 1 B). The inverse is also possible. A response can be conditionally dependent on a predictor, but marginally independent when another response has a similar dependence with that predictor (Figure 1 F). In this case, the link between the responses could marginally cancel out the effect of the predictor.

Here, we introduce a model framework to infer a sparse network structure that represents both interactions among responses and effects of a set of predictors. Specifically, our model estimates a network that represents the conditional dependence structure of a multivariate response (e.g. abundances of microbes) while simultaneously estimating the conditional effect of a set of predictors that influence the network (e.g. diet, weather, experimental treatments). Our model is represented by a chain graph ([Lauritzen and Wermuth, 1989](#); [Lauritzen and Richardson, 2002](#)) with two sets of nodes: predictors and responses (Figure 1). Directed edges between a predictor and a response represent conditional links, and undirected edges among responses represent correlations. While chain graph models are not new, we can argue that they are under-utilized in microbiome studies and our work will serve to illustrate its potential to elucidate ties between microbial interactions and experimental or environmental predictors.

In addition to providing a more sensible representation compared to standard multiresponse linear regression, our model guarantees a sparse solution via Bayesian LASSO, and we show that this sparse solution is guaranteed to be the sparse solution of the Conditional Auto-Regressive (CAR) model ([Ver Hoef et al., 2018](#)). Furthermore, we propose an adaptive extension that allows different shrinkage to different edges to incorporate edge-specific knowledge into the model, and we use the Normal model as a core and build hierarchical structures upon it to account for binary, counting and compositional responses. Finally, our model is able to equally handle small and big data and is computationally inexpensive through an efficient Gibbs sampling algorithm.

2 Methods

2.1 Model specification

Let $\mathbf{Y}_i \in \mathbb{R}^k$ be a multivariate response with k entries for $i = 1, \dots, n$ observations. Let $\mathbf{X}_i \in \mathbb{R}^{1 \times p}$ be the row vector of predictors for $i = 1, \dots, n$ (i.e. the i^{th} row of the design matrix $\mathbf{X} \in \mathbb{R}^{n \times p}$). We assume that the design matrix is standardized so that each column has a mean of 0 and same standard deviation (set to be 1 in the simulations) so that same shrinkage parameter will not have different effect on different predictors.

Let \mathbf{Y}_i follow a Normal distribution with mean vector $\mathbf{B}^T \mathbf{X}_i^T + \mu$ and precision matrix $\mathbf{\Omega} \in \mathbb{R}^{k \times k}$ (positive definite) where $\mathbf{B} \in \mathbb{R}^{p \times k}$ corresponds to the regression coefficients connecting the responses ($\mathbf{Y}_i \in \mathbb{R}^k$) and the predictors ($\mathbf{X}_i \in \mathbb{R}^{1 \times p}$) and $\mu \in \mathbb{R}^k$ corresponds to the intercept. We use the transpose $\mathbf{B}^T \mathbf{X}_i^T \in \mathbb{R}^{k \times 1}$ because samples are encoded as row vectors in the design matrix while by convention multivariate Normal samples are column vectors.

The likelihood function of the model is:

$$p(\mathbf{Y}_i | \mathbf{X}_i, \mu, \mathbf{B}, \mathbf{\Omega}) \propto \exp[(\mathbf{B}^T \mathbf{X}_i^T + \mu)^T \mathbf{Y}_i - \frac{1}{2} \mathbf{Y}_i^T \mathbf{\Omega} \mathbf{Y}_i]. \quad (1)$$

Note that in this parametrization, \mathbf{B} encodes *conditional dependence* between \mathbf{Y} and \mathbf{X} because in the kernel of the density, B_{ij} is the coefficient of product between X_i and Y_j . Thus, if $B_{ij} = 0$, then X_i and Y_j are *conditionally independent*. This is analogous to the case of $\mathbf{\Omega}$ whose off-diagonal entries encode the conditional dependence between responses Y_i and Y_j .

From a graphical perspective, \mathbf{B} represents the adjacency matrix between response nodes (\mathbf{Y}) and predictor nodes (\mathbf{X}) while the off-diagonal entries of $\mathbf{\Omega}$ represent the partial correlations which coincide with the adjacency matrix between response nodes. The parameter estimations of \mathbf{B} and $\mathbf{\Omega}$ are indeed adjacency matrices of a chain graph ([Andersson et al., 2001](#); [Lauritzen and Wermuth, 1989](#); [Frydenberg, 1990](#))

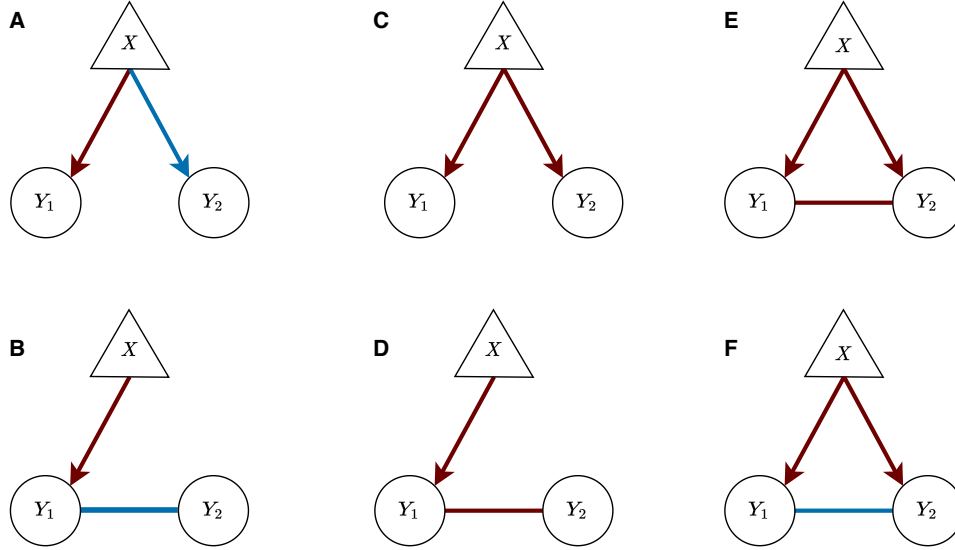


Figure 1: **Simple networks with predictors.** We use a triangle to represent a predictor X and circles to represent the responses Y_1 and Y_2 . Red edges correspond to positive links between nodes while blue edges correspond to a negative links. Networks A and B (likewise networks C and D) can produce a similar marginal correlation structure between any two nodes. Distinguishing edges in E can be difficult since all edges have the same direction. Finally, in network F, X and Y_2 are conditionally correlated, yet they might not have a marginal correlation. For example, if Y_1, Y_2 had marginal variance 1 and covariance $\rho = -0.5$, while the conditional regression coefficient between Y_1 and X conditioned on Y_2 was $\beta_1 = 2 > 0$ and conditional regression coefficient between Y_2 and X conditioned on Y_1 was $\beta_2 = 1 > 0$, we can show that the marginal regression coefficient between Y_2 and X when integrating out Y_1 is $\rho\beta_1 + \beta_2 = 0$ (more in Section 2.2).

2.1.1 Correspondence to classical CAR

The parameters in the proposed model corresponds to a scale transformation of the classical conditional auto-regressive (CAR) model (Ver Hoef et al., 2018), and both models share sparse solutions. We can re-parametrize our model to the classical CAR parametrization as follows. Let \mathbf{B}' denote the unscaled conditional regression coefficients between responses and predictors. Let \mathbf{C} denote the conditional regression coefficients between responses, and let \mathbf{M} denote the conditional variance. We can generate the three matrices by decomposing $\mathbf{\Omega}$. Define diagonal matrix \mathbf{D} by $\mathbf{D}_{ii} = \mathbf{\Omega}_{ii}$ and $\mathbf{R} = \mathbf{D} - \mathbf{\Omega}$. Then we can calculate $\mathbf{C} = \mathbf{D}^{-1}\mathbf{R}$, $\mathbf{M} = \mathbf{D}^{-1}$ and $\mathbf{B}' = \mathbf{D}^{-1}\mathbf{B}$ (Ver Hoef et al., 2018). Though a sparse precision matrix ($\mathbf{\Omega}$) guarantees a sparse conditional auto-regression coefficient (\mathbf{C}), one needs to be careful about the negative sign in this transformation. Conditional auto-regression coefficients (\mathbf{C}) have opposite signs to those in the precision matrix ($\mathbf{\Omega}$).

2.1.2 Prior specification

We assume a Laplace prior on the entries of \mathbf{B} and graphical LASSO prior on $\mathbf{\Omega}$ (Park and Casella, 2008; Wang, 2012). Using the Normal scale mixture representation of Laplace distribution (Park and Casella, 2008; Wang, 2012; Andrews and Mallows, 1974), let η_{ml} be the latent scale parameters for $\mathbf{\Omega}$ for $1 \leq m < l \leq k$ since $\mathbf{\Omega}$ is symmetric and let τ_{ij} ($1 \leq i \leq p, 1 \leq j \leq k$) be the latent scale parameters for \mathbf{B} .

The full model specification is then:

$$\begin{aligned}
\mathbf{Y}_i | \mathbf{X}_i, \mu, \mathbf{B}, \boldsymbol{\Omega} &\sim N(\boldsymbol{\Omega}^{-1}(\mathbf{B}^T \mathbf{X}_i^T + \mu), \boldsymbol{\Omega}^{-1}) \\
B_{ij} | \tau_{ij} &\sim N(0, \tau_{ij}^2) \\
\tau_{ij} &\sim \frac{\lambda_\beta^2}{2} e^{-\lambda_\beta^2 \tau_{ij}} \\
p(\boldsymbol{\Omega} | \boldsymbol{\eta}, \lambda_\Omega) &= C_\eta^{-1} \prod_{m < l} \left[\frac{1}{\sqrt{2\pi\eta_{ml}}} \exp\left(-\frac{\omega_{ml}^2}{2\eta_{ml}}\right) \right] \prod_{m=1}^k \left[\frac{\lambda_\Omega}{2} \exp\left(-\frac{\lambda_\Omega \omega_{mm}}{2}\right) \right] I_{\boldsymbol{\Omega} \in M^+} \\
p(\boldsymbol{\eta} | \lambda_\Omega) &\propto C_\eta \prod_{m < l} \frac{\lambda_\Omega^2}{2} \exp\left(-\frac{\lambda_\Omega^2 \eta_{ml}}{2}\right)
\end{aligned} \tag{2}$$

where $I_{\boldsymbol{\Omega} \in M^+}$ means that $\boldsymbol{\Omega}$ must be positive definite.

2.2 On conditional (in)dependence

In regression models for multivariate response, the regression coefficients linking a given response with the predictors can be conditional (conditioned on the other responses) or marginal (integrating out the other responses). In our model, the regression coefficients matrix \mathbf{B} encode conditional dependence (scaled by marginal variance) between the responses and the predictors which coincides with the chain graphical model (Andersson et al., 2001; Lauritzen and Wermuth, 1989; Frydenberg, 1990).

Biologically, conditional regression coefficients are more interpretable than marginal regression coefficients (recall the example that penicillin has no effect on Gram-negative microbes). In particular, given prior knowledge on the behavior of microbes (e.g. laboratory controlled experiments), it is crucial for the regression coefficients to encode *conditional* dependence between nodes and predictors or the biological prior knowledge would be misused. For instance, our prior knowledge on "penicillin does not have an effect on Gram-negative microbes" should be encoded as conditional independence rather than marginal since penicillin would reduce competition from Gram-positive microbes.

Despite its biological interpretability, there are downsides to a conditional construction. For example, with conditional coefficients is not possible to do marginal predictions of nodes given that the marginal distribution depends on the regression coefficients of other nodes as well as on the covariance matrix.

In general, it is not possible to find sparse marginal prediction of single node and sparse graphical selection simultaneously. That is, for $\tilde{\mathbf{B}} = \mathbf{B}\boldsymbol{\Omega}^{-1}$, marginal prediction requires that $\tilde{\mathbf{B}}$ encodes *marginal* dependence to predictors so that we can take a certain column and use it like the regression coefficient of that single node. On the contrary, graphical selection requires that \mathbf{B} encodes *conditional* dependence. Simultaneous marginal prediction and graphical selection is only possible when $\boldsymbol{\Omega}^{-1}$ is diagonal so that both \mathbf{B} and $\tilde{\mathbf{B}}$ can be sparse, i.e. when nodes are independent, and thus, $B_{ij} = 0$ implies $\tilde{B}_{ij} = 0$ for any \mathbf{B} .

Our model focuses on graphical selection, yet we also implement a model for sparse marginal regression coefficient and sparse precision matrix by combining the Gibbs sampling for the precision matrix in Wang (2012) with the Gibbs sampler in Park and Casella (2008). We denote this model Simultaneous Regression and Graphical LASSO (SRG-LASSO) and we use it to compare to the CAR-LASSO in the simulation study (Section 3).

2.3 Implementation

2.3.1 Sampling scheme

We derive an efficient Gibbs sampler for all parameters in this model due to the scale mixture representation of the graphical LASSO prior (Wang, 2012). Details on derivation of the sampling scheme can be found in the Appendix and are summarized in Algorithm 1 with all the extensions (Section 2.4).

2.3.2 Choice of hyperparameters

The shrinkage parameters λ_Ω and λ_β (Equation 2) are hyperparameters to be determined. As in Park and Casella (2008); Wang (2012), we assume these shrinkage parameters have a hyperprior Gamma distribution with shape parameter r and rate parameter δ which can be set to produce a relatively flat density for a non-informative prior scenario. Note that since the prior on $\boldsymbol{\Omega}$ is not a Laplace but a graphical LASSO prior (Wang, 2012), the Gamma prior is on λ , not on λ^2 as

Algorithm 1: Implementation of Gibbs sampling**Result:** MCMC samples of the posterior distribution of parameters of interest

Initialization;

while not enough samples **do** **if** responses not Normal **then**

Update the latent Normal variables using Adaptive Rejection Sampling (ARS) for counting and compositional data and truncated Normal for binary data (Section 2.4.2);

end **for** i^{th} diagonal entries in Ω **do** /* blockwise update for Ω */ Sample the determinant of Ω : $\gamma | \Omega_{[i]}, \eta, \lambda_\Omega \sim$ Generalize Inverse Gaussian (GIG) distribution (Equation A3) where $\Omega_{[i]}$ corresponds to some partition of Ω based on the diagonal entry ω_{ii} ; Update the off diagonal entries in the i^{th} row (column): $\omega_{-ii} | \gamma, \Omega_{[i]}, \eta, \lambda_\Omega \sim$ Normal distribution (Equation A4); Compute the updated i^{th} diagonal entry (ω_{ii}) with Equation A2 that depends on the determinant (γ), the off diagonal entries (ω_{-ii}) and the partition of Ω ($\Omega_{[i]}$); **end** Update $\mathbf{B} | \tau^2, \Omega, \mu, \mathbf{X}, \mathbf{Y} \sim$ Normal distribution (Equation A6); Update $\mu \sim \text{Normal}((\mathbf{Y}\Omega - \mathbf{X}\mathbf{B})^T, \Omega/n)$; Update latent variables in the scale mixture representation of the two LASSO priors: $\eta = \{\eta_{jk}\}, \tau = \{\tau_{jk}\}$ following an Inverse Gaussian distribution (Equation A5); **if** adaptive shrinkage **then** Update the shrinkage parameters on Ω ($\lambda_{jk,\Omega}$) and on \mathbf{B} ($\lambda_{jk,\beta}^2$) for individual entries (Section 2.4.1); **else** Update the shrinkage parameters on Ω (λ_Ω) and on \mathbf{B} (λ_β^2) uniformly for all entries following a Gamma distribution (Section 2.3.2); **end****end**

it would be under a Laplace prior.

$$\lambda_\beta^2 \sim \text{Gamma}(r_\beta, \delta_\beta)$$

$$\lambda_\Omega \sim \text{Gamma}(r_\Omega, \delta_\Omega)$$

The shrinkage parameters λ_Ω and λ_β are included in the Gibbs sampler with full conditional distribution still Gamma with shape parameters $r_\beta + kp, \delta_\beta + \sum \tau_i/2$ and rate parameters $r_\Omega + k(k+1)/2, \delta_\Omega + \|\Omega\|_1/2$ respectively.

2.3.3 Learning the graphical structure

Our model has a zero posterior probability for a parameter to be zero given the continuous priors. Yet, we still need to determine the cases when the edges of the graph will be considered "non-existent". Here, we infer the graph structure using the horseshoe method in [Carvalho et al. \(2010\)](#); [Wang \(2012\)](#) which compares the LASSO estimate for the regression coefficient with the posterior mean of a standard conjugate (non-shrinkage) prior ([Jones et al., 2005](#)).

Let $\pi = \frac{\tilde{\theta}}{E_g(\tilde{\theta} | \mathbf{Y})}$ where $\tilde{\theta}$ represents the estimate of the parameter under the LASSO prior and $E_g(\theta | \mathbf{Y})$ is the posterior mean of that parameter under non-shrinkage prior (e.g. Normal for \mathbf{B} and Wishart for Ω). The statistics $1 - \pi$ characterizes the amount of shrinkage due to the LASSO prior. We use $\pi > 0.5$ as the threshold to decide that $\theta \neq 0$ as in [Wang \(2012\)](#).

2.4 Extensions

2.4.1 Adaptive LASSO

One simple extension to LASSO is Adaptive LASSO, in which the shrinkage parameter λ can be different for all elements in \mathbf{B} and Ω ([Leng et al., 2014](#); [Wang, 2012](#)). This extension is particularly useful when we have prior knowledge of independence among certain nodes. For example, larger shrinkage parameters (λ) on specific entries can be used to indicate prior knowledge of independence.

As suggested in [Leng et al. \(2014\)](#); [Wang \(2012\)](#), we set the hyperpriors on $\lambda_{ij,\beta}^2$ as Gamma distributions with shape parameters $r_{ij,\beta}$ and rate parameter $\delta_{ij,\beta}$. We also set the prior suggested in [Wang \(2012\)](#) for $\lambda_{ij,\Omega}$ (with $i \neq j$). While in [Wang \(2012\)](#) shrinkage on diagonal $\lambda_{ii,\Omega}$ is a hyperparameter, we set it here to 0. That is, we are not shrinking the diagonal entries of Ω . But such shrinkage can be included by multiplying the prior of Ω by $\prod_{i=1}^k \frac{\lambda_{ii}}{2} \exp(-\lambda_{ii,\Omega} \omega_{ii})$.

The prior for Ω is

$$p(\Omega | \{\lambda_{ij,\Omega}\}_{i < j}) = C_{\{\lambda_{ij,\Omega}\}_{i < j}}^{-1} \prod_{i < j} \frac{\lambda_{ij,\Omega}}{2} \exp(-\lambda_{ij,\Omega} |\omega_{ij}|) I_{\Omega \in M_+}$$

$$p(\{\lambda_{ij,\Omega}\}_{i < j}) \propto C_{\{\lambda_{ij,\Omega}\}_{i < j}} \prod_{i < j} \frac{1}{\Gamma(r_{ij,\Omega})} \lambda_{ij,\Omega}^{r_{ij,\Omega}-1} \exp(-\delta_{ij,\Omega} \lambda_{ij,\Omega}).$$

The full conditional distribution of the shrinkage parameters is then Gamma (shape and rate parametrization):

$$\lambda_{ij,\Omega} | \Omega \sim \text{Gamma}(r_{ij,\Omega} + 1, \delta_{ij,\Omega} + |\omega_{ij}|), i \neq j$$

$$\lambda_{ij,\beta}^2 | \tau \sim \text{Gamma}(r_{ij,\beta} + 1, \delta_{ij,\beta} + \tau_{ij}/2).$$

We set the hyperparameters as $r = 10^{-2}$ and $\delta = 10^{-6}$ for both Ω and \mathbf{B} ([Wang, 2012](#); [Leng et al., 2014](#)) with a small value of δ selected to take advantage of the adaptiveness of the shrinkage.

2.4.2 Other types of responses

The model has been defined for continuous responses, yet there are different extensions for the case of binary data, counts and compositional data that we describe below.

- *Probit model for binary data.* For binary responses, we can use a Probit model with CAR in the core of the dependence structure. We denote the CAR latent variable as $\mathbf{Z}_i \in \mathbb{R}^k$, and let $\Phi(Z_{ij})$ model the probability of observing a 1 where Φ is the cumulative distribution function of a standard Normal. Equation 3 shows the alternative representation of the model:

$$\begin{aligned} \mathbf{Z}_i &\sim N(\Omega^{-1}(\mathbf{B}^T \mathbf{X}_i^T + \mu), \Omega^{-1}) \\ Y_{ij}^* &\sim N(Z_{ij}, 1) \\ Y_{ij} &= \mathbf{1}_{Y_{ij}^* > 0} \end{aligned} \quad (3)$$

Then, the full conditional probability of Y_{ij}^* is a truncated Normal with mean Z_{ij} and variance 1. By denoting $\hat{\mu}_i = (\mathbf{B}^T \mathbf{X}_i^T + \mu)$, we have the full conditional distribution of \mathbf{Z}_i :

$$\mathbf{Z}_i | Y_i^*, \hat{\mu}_i, \Omega \sim N([\Omega + I]^{-1}(\hat{\mu}_i + Y_i^*), [\Omega + I]^{-1}).$$

- *Log-normal Poisson model for counts.* To model a response of multivariate counts, we use a Lognormal-Poisson model ([Aitchison and Ho, 1989](#)). Let $\mathbf{Z}_i \in \mathbb{R}^k$ be the latent vector of log expected counts of the i^{th} sample and let $\mathbf{Y}_i \in \mathbb{N}^k$ be the observed counts. We use $\mathbf{Z}_{i,-j} \in \mathbb{R}^{k-1}$ to denote the vector of log expected counts of the i^{th} sample but without response j and Z_{ij} as the log expected counts of the i^{th} sample and j^{th} response.

The covariance matrix accounts for both over-dispersion and correlation of the counts:

$$\begin{aligned} \mathbf{Z}_i &\sim N(\Omega^{-1}(\mathbf{B}^T \mathbf{X}_i^T + \mu), \Omega^{-1}) \\ \lambda_{ij} &= \exp(Z_{ij}) \\ Y_{ij} &\sim \text{Poisson}(\lambda_{ij}). \end{aligned} \quad (4)$$

Then, the density of Y_{ij} is:

$$p(Y_{ij} | Z_{ij}) \propto \exp\{Y_{ij} Z_{ij} - e^{Z_{ij}}\}.$$

Let $Z_{ij} | \mathbf{Z}_{i,-j} \sim N(\tilde{\mu}_{ij}, \tilde{\sigma}_{ij}^2)$ be the conditional prior so that the log full conditional is:

$$\log[p(Z_{ij} | \mathbf{Z}_{i,-j}, \hat{\mu}, \Omega, Y)] = Y_{ij} Z_{ij} - \exp(Z_{ij}) - \frac{1}{2\tilde{\sigma}_{ij}^2} (Z_{ij} - \tilde{\mu}_{ij})^2 + C$$

which is concave. This means that we can sample the full conditional distribution of the latent variables using adaptive rejection sampling (ARS) (Gilks and Wild, 1992), and this can be done in parallel to further speed up the sampling.

- *Normal-Logistic for multinomial data.* As in Xia et al. (2013), we develop a Normal-Logistic model for multinomial compositional data. This type of data is very common in microbiome and ecology studies.

Assume that we have $k + 1$ responses in our sample and the last response serves as reference group. Let $\mathbf{Z}_i \in \mathbb{R}^{k+1}$ denote the latent vector of logit transformed relative abundances for i^{th} sample, and let $\mathbf{Y}_i \in \mathbb{N}^k$ be the observed species counts. Denote as M the known total count (e.g. sequence depth in microbiome studies). Similarly we use $\mathbf{Z}_{i,-j}$ to denote the vector logit transformed relative abundance of the i^{th} sample but without response j and Z_{ij} as the log expected counts of the i^{th} sample and j^{th} response.

The Normal-Logistic model has the following structure:

$$\begin{aligned} \mathbf{Z}_i &\sim N(\mathbf{\Omega}^{-1}(\mathbf{B}^T \mathbf{X}_i^T + \mu), \mathbf{\Omega}^{-1}) \\ p_{ij} &= \frac{\exp(Z_{ij})}{\sum_{i=1}^k \exp(Z_{ij}) + 1} \\ \mathbf{Y}_i &\sim \text{Multinomial}(p_{i1}, \dots, p_{ik}, M) \end{aligned} \quad (5)$$

Note that the Normal latent variables take care of the over-dispersion.

Then, the likelihood of \mathbf{Y}_i is:

$$p(\mathbf{Y}_i | \mathbf{Z}_i) = \frac{1}{\sum_{j=1}^k \exp(Z_{ij}) + 1} \prod_{j=1}^k \frac{\exp(Y_{ij} Z_{ij})}{\sum_{j=1}^k \exp(Z_{ij}) + 1}$$

Let $Z_{ij} | \mathbf{Z}_{i,-j} \sim N(\tilde{\mu}_{ij}, \tilde{\sigma}_{ij}^2)$ be the conditional prior so that the log full conditional is:

$$\log[p(Z_{ij} | \mathbf{Z}_{i,-j}, \hat{\mu}, \Omega, Y)] = Y_{ij} Z_{ij} - N \log \left(\sum_{j=1}^k \exp(Z_{ij}) + 1 \right) - \frac{1}{2\tilde{\sigma}_{ij}^2} (Z_{ij} - \tilde{\mu}_{ij})^2 + C$$

This function is concave because the first term is an affine, the second term is the negative log sum of exponential of an affine function, and the last term is a concave quadratic form. Thus, ARS (Gilks and Wild, 1992) can again be used during the Gibbs sampling, and this process can be parallelized for extra speed.

3 Simulation studies

3.1 Simulation design

We simulate data under the six graphical structures in Wang (2012) with a multivariate response of dimension $k = 10, 30$, $p = 5, 10$ predictors and $n = 50$ samples. We vary the sparsity of \mathbf{B} with 80% or 50% entries equal to zero (denoted beta sparsity of 0.8 and 0.5 in the figures) and a grand mean (i.e. intercept μ) of 0. Design matrices are sampled from standard Normal distributions. Each simulation setting was repeated 50 times.

The six graphical structures are defined below and in Figure 2. Note that model 1 and model 3 specify the entries of the covariance matrix Σ (σ_{ij}) while the other models specify the entries of the precision matrix Ω (ω_{ij}).

- Model 1: An AR(1) model with $\sigma_{ij} = 0.7^{|i-j|}$
- Model 2: An AR(2) model with $\omega_{ii} = 1$, $\omega_{i-1,i} = \omega_{i,i-1} = 0.5$, $\omega_{i-2,i} = \omega_{i,i-2} = 0.25$ for $i = 1, \dots, k$
- Model 3: A block model with $\sigma_{ii} = 1$ for $i = 1, \dots, k$, $\sigma_{ij} = 0.5$ for $1 \leq i \neq j \leq k/2$, $\sigma_{ij} = 0.5$ for $k/2 + 1 \leq i \neq j \leq 10$ and $\sigma_{ij=0}$ otherwise.
- Model 4: A star model with every node connected to the first node, with $\omega_{ii} = 1$, $\omega_{1,i} = \omega_{i,1} = 0.1$ for $i = 1, \dots, k$, and $\omega_{ij} = 0$ otherwise.
- Model 5: A circle model with $\omega_{ii} = 2$, $\omega_{i-1,i} = \omega_{i,i-1} = 1$ for $i = 1, \dots, k$, and $\omega_{1,j} = \omega_{j,1} = 0.9$ for $j = 1, \dots, k$.
- Model 6: A full model with $\omega_{ii} = 2$ and $\omega_{ij} = 1$ for $i \neq j \in \{1, \dots, k\}$.

On the simulated data, we compare the performance of 12 methods:

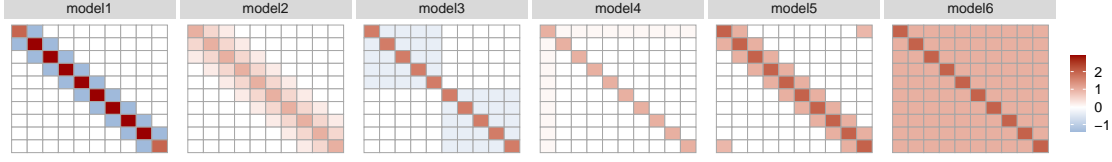


Figure 2: Precision matrices Ω used in the simulations for a multivariate response of dimension $k = 10$. These six models correspond to the six graphical structures in Wang (2012). Red corresponds to a positive entry and blue corresponds to a negative entry. Note that the colors are the inverse of the correlations.

1. CAR-LASSO: our proposed model
2. Adaptive CAR-LASSO: our proposed model with different shrinkage parameters for different entries in \mathbf{B} and Ω
3. SRG-LASSO: our model focused on marginal prediction described in Section 2.2
4. Graphical LASSO in Wang (2012)
5. Adaptive Graphical LASSO: adaptive version in Wang (2012)
6. Augmented Graphical LASSO: Graphical LASSO including responses and predictors (assumed Normally distributed). In this case, we consider separately the sub-graphs corresponding to \mathbf{B} and Ω
7. Adaptive version of Augmented Graphical LASSO
8. Bayesian multiresponse regression with conjugate priors. Since this model does not really estimate the conditional regression coefficients \mathbf{B} but the marginal regression coefficient $\tilde{\mathbf{B}}$, we get $\mathbf{B} = \tilde{\mathbf{B}}\Omega$ (see Section 2.2)
9. Bayesian multiresponse regression with conjugate priors that assume the marginal mean is 0 (similar to Graphical LASSO)
10. Bayesian multiresponse regression with conjugate priors that assume the marginal mean is 0 (similar to Graphical LASSO), but using all the responses and predictors as "responses" in the model
11. Calculate the empirical covariance matrix and take inverse (denoted ad-hoc in the figures)
12. Calculate the empirical covariance matrix with both responses and predictors and take inverse (denoted ad-hoc-aug in the figures)

As in Wang (2012); Leng et al. (2014), we set the hyperparameters of the Gamma hyperprior for the shrinkage parameters of both \mathbf{B} and Ω as $r = 0.01$, $\delta = 10^{-6}$ for the adaptive versions, and $r = 1$, $\delta = 0.01$ for the non-adaptive versions. In the multiresponse regression models (methods 9 and 10), we consider any edge with weight $< 1 \times 10^{-3}$ to be 0.

To evaluate the performance of the methods, we compute the L2-loss of the estimate of \mathbf{B} and the Stein's loss of the estimate of Ω . We use Stein's loss for Ω since it is the KL-divergence when the mean vector is 0. In addition, we evaluate the reconstruction of the graphical structures based on the Matthews Correlation Coefficient (MCC) (Fan et al., 2009) which range from -1 to 1 with 1 representing a perfect prediction.

Finally, we calculated the proportion of true positive edges and false positive edges in the reconstructed graph (Ω). The true positive rate is calculated as the proportion of times a true edge is reconstructed and the false positive rate is calculated as the proportion of times an edge appears in the estimated graph that is not present in the true graph. The false positive rate is presented as a negative quantity aligned with other network reconstruction practice (Xie et al., 2021). Given that the covariance model 6 is a fully connected graph (and thus, there are no true negatives or false positives), we did not calculate the MCC nor the true/false positive rates in this case.

3.2 Simulation results

Our proposed models (CAR-LASSO and adaptive CAR-LASSO) outperform the other models in almost every covariance model and sparsity setting with the adaptive version outperforming the non-adaptive version in almost every setting in reconstructing the precision matrix evaluated by Stein's loss (Figure A1 for $k = 30$ nodes and Figure A5 for $k = 10$ nodes). Similarly, our proposed models (CAR-LASSO and adaptive CAR-LASSO) outperform the other models in almost every covariance model and sparsity setting in reconstructing the regression coefficient matrix evaluated by L2

loss (Figure A2 for $k = 30$ nodes and Figure A6 for $k = 10$ nodes). However, unlike in the case of Ω , the adaptive version did not outperform the non-adaptive version in some scenarios especially when \mathbf{B} is not sparse. Note that Graphical LASSO and Adaptive Graphical LASSO are not included in this plot because these models do not estimate the matrix of regression coefficients \mathbf{B} .

In all cases, adaptive CAR-LASSO has the highest MCC in both the estimation of the precision matrix and the regression coefficients. For precision matrix, see Figure A3 ($k = 30$ nodes) and Figure A7 ($k = 10$ nodes). For regression coefficients, see Figure A4 ($k = 30$ nodes) and Figure A8 ($k = 10$ nodes). Covariance model 4 is an exception where all methods performed poorly in the estimation of Ω (Figures A3 and A7, MCC around 0 in all cases). In model 4, the off diagonal signal is weak compared to other models (off diagonal entries close to 0.1 while diagonal entries are close to 1). It is also the sparsest setting with 80% of off diagonal entries to be 0 when $k = 10$ and 93% when $k = 30$ (Figure 2). This setup might cause penalized methods to over penalize the off diagonal entries.

It is worth noting that Augmented Graphical LASSO also shows good performance in most cases. However, this method assumes that the joint distribution of responses and predictors is Normal. This is the case in our simulation setup, and hence, the good performance of the method. However, our CAR-LASSO model is more flexible because does not make any assumptions on the design matrix. We also find that the Adaptive Graphical LASSO tends to over penalize and produce estimations that are close to the diagonal in most simulation settings.

Lastly, we select the four best performing methods based on MCC plus Bayesian multiresponse linear regression as a reference (model 8) to plot the true/false positive rates in the estimation of edges. Figure 3 shows the results for case of the precision matrix (Ω) under the simulation setting of $k = 10$ nodes, $p = 10$ predictors and sparsity level of 0.8. Adaptive CAR-LASSO (CAR-A) produces the lowest false positive rate (represented as blue entries). In contrast, Bayesian multiresponse linear regression (multireg) has a high false positive rate because it is not enforcing any sparsity in the graph. The good performance of Adaptive CAR-LASSO is corroborated on the other simulation settings: Figure A9 for $k = 10, p = 5$ and sparsity of 0.8, Figure A10 for $k = 10, p = 5$ and sparsity of 0.5 and Figure A11 for $k = 10, p = 10$ and sparsity of 0.5.

Figure 4 shows the results for case of the regression coefficients (\mathbf{B}) under the same simulation setting of $k = 10$ nodes, $p = 10$ predictors and sparsity level of 0.8. Similarly, Adaptive CAR-LASSO (CAR-A) produces the lowest false positive rate (represented as blue entries) compared to the other good performing methods. The good performance of Adaptive CAR-LASSO is corroborated on the other simulation settings: Figure A12 for $k = 10, p = 5$ and sparsity of 0.8, Figure A13 for $k = 10, p = 5$ and sparsity of 0.5 and Figure A14 for $k = 10, p = 10$ and sparsity of 0.5.

3.3 Computational speed and scaling

We test the scalability of our estimation procedure by simulating 500 and 1000 samples with 5, 10, 25, 50, 100 nodes. We sample 1000 generations with 100 burn-in on a machine with Core-i7 4790 CPU and Windows 7 operating system. We recorded CPU seconds in R.

While our models are slower than Graphical LASSO or multiresponse regression, running time is not severely impacted by sample size (Figure 5). Instead, speed is mostly influenced by the number of nodes and the number of predictors. However, even the case of 100 nodes and 10 predictors is successfully completed in less than 10 minutes.

4 Application to real microbiota data

4.1 Human gut microbiota compositional data

The microbiota of older people displays greater inter-individual variation than that of younger adults. The study in Claesson et al. (2012) collected faecal microbiota composition from 178 elderly subjects, together with subjects' residence type (in the community, day-hospital, rehabilitation or in long-term residential care) and diet (data at O'Toole (2008)). Researchers studied the correlation between microbes and other measurements. They found that individual microbiota of people in long-stay care was significantly less diverse and loss of diversity might associate with increased frailty. They clustered microbes based on co-abundances and performed dimension reduction techniques to infer relationships between composition and health. However co-abundances might not appropriately infer interactions because of the existence of other microbes and environment (Blanchet et al., 2020). Partial correlations between microbes and environment or other microbes are more ecologically meaningful. Here, we infer the partial correlation between environments and among microbes in those elderly subjects by reconstructing a sparse network via the adaptive CAR-LASSO model.

We use the MG-RAST server (Meyer et al., 2008) for profiling with an e-value of 5, 60% identity, alignment length of 15 bp, and minimal abundance of 10 reads. Unclassified hits are not included in the analysis. Genus with more than

0.5% (human) or 1% (soil) relative abundance in more than 50 samples is selected as the focal genus and all other genus serve as the reference group.

We reconstruct the weighted graph using the conditional regression coefficient between any two nodes. The α -centrality (Bonacich and Lloyd, 2001) is used to identify the importance of nodes. Weighted adjacency matrix is constructed with the posterior mean of the conditional regression coefficients of those that showed significance with the horseshoe method described in Section 2.3.3.

Figure 6 shows the estimated human gut microbiota network under the adaptive CAR-LASSO model where the edges with the most weight correspond to connections between genus nodes, not so much with predictors. The most important predictor is whether the patient’s residence was a long-term residential care which positively affected genus *Caloramator*. This result agrees with the original analysis that also separated elderly subjects based upon where they live in the community. Another important predictor is Diet Group 4 which corresponds to the high fat/low fiber group. This diet positively affected genus *Caloramator* as well.

4.1.1 Comparison with a marginal network

As comparison, we estimate the marginal network (Figure 7) to observe the differences with the conditional network in Figure 6. To obtain the marginal network, we start with the conditional network and use the equivalence $\tilde{\mathbf{B}} = \mathbf{B}\mathbf{\Omega}^{-1}$ in Section 2.2. Edges between predictors and responses are marginal regression coefficients while edges between responses are covariances. Edges between responses and predictors generally agree within two cases given the partial correlation between responses are mostly positive (Figure 7). However, marginally the connection between responses and predictors is very dense. This is because all responses (genus) are connected by their partial correlations so that as long as the predictor can influence one of the responses conditionally, it should be able to affect all the responses marginally. We observe that some edges flip color when comparing the conditional and the marginal network. For example, the link between Diet Group 2 corresponding to both complex (wholegrain breakfast cereals and breads, boiled potatoes) and simple carbohydrates (white bread) and *Veillonella* is blue (negative) in the conditional network (Figure 6) and red (positive) in the marginal network (Figure 7). *Veillonella* is well known for its lactate fermenting abilities, so a negative link with a carbohydrate diet is reasonable. Edges flipping color could be explained by interactions with other genus. Another example is that marginally, all links are blue (negative) from Diet Group PEG (percutaneous endoscopic gastrostomy (PEG)-fed subjects) to the genus whereas conditionally there is a positive (red) link with *Parabacteroides*. These observations further reiterate that we should distinguish marginal and conditional effects of predictors in these research scenarios, especially when sparsity is assumed since it is usually impossible to have both marginal and conditional effects sparse.

4.2 Soil microbiota compositional data

The objective of this study (Hofmockel, 2012; Bach et al., 2018) is to examine soil microbial community composition and structure of both bacteria and fungi at a microbially-relevant scale. The researchers isolated soil aggregates from three land management systems in central Iowa to test if the aggregate-level microbial responses are related to plant community and management practices. The clean dataset has 120 samples with 17 genus under consideration. We focus on the bacteria to further evaluate the partial association among them and the environmental factors.

We use the MG-RAST server (Meyer et al., 2008) with the same settings as in the human gut microbiome data described in Section 4.1. In addition, weighted adjacency matrix is also constructed with the posterior mean of the conditional regression coefficients of those that showed significance with the horseshoe method described in Section 2.3.3.

Figure 8 shows the soil microbiota estimated network using the adaptive CAR-LASSO model. In this network, the most important link is between *Candidatus Solibacter* and *Candidatus Koribacter*. There are not important connections with predictors in this case which seem to suggest that the soil microbial community is robust to environmental perturbations. These results agree with the original research that indicated that core microbial communities within soil aggregates are likely driven by stable and long-term factors such as clay content rather than relative short time scaled land management as the ones considered as predictors in this study. We note that the original research concentrated on the diversity of the community while our analysis focuses on the structure and correlations within the community.

4.2.1 Comparison with a marginal network

Again, we estimate the marginal network (Figure 9) starting with the conditional network and using the equivalence $\tilde{\mathbf{B}} = \mathbf{B}\mathbf{\Omega}^{-1}$ in Section 2.2. Edges between predictors and responses are marginal regression coefficients while edges between responses are covariances. In the estimated network (Figure 9), we see a much stronger marginal effect of environmental predictors than the one we had seen with conditional effects (Figure 8). The LASSO penalty

might contribute to this behavior, but it might also be because the observed strong dependence between microbes and environment is due to the strong partial correlation among microbes. In addition, marginally, crop agriculture and total nitrogen (total N) have strong correlations to multiple genus. However, this pattern is not obvious in the conditional network (nor on the original research). It might suggest that the influence of crop agriculture and total N might be enhanced by strong partial correlation among microbes. The largest partial regression coefficient for total N is to genus *Nitrososphaera* which is indeed a N-fixing genus and it has the highest α -centrality (Fig.10).

To conclude, the marginal network does not agree with the original research that core microbial communities within soil aggregates are likely driven by stable and long-term factors instead of the predictors measured in the data. Unlike marginal effects, conditional effects of the environment can be more informative to biologists who would like to conduct research in understanding the environment's effect on certain microbes, for instance, the effect of environmental antibiotics.

It is worth highlighting that our model can produce meaningful results from relative small sample sizes: 120 samples for the soil microbiota study and 178 samples for the human gut microbiota study.

4.3 Comparison of α -centrality and abundances in human and soil communities

We evaluated the α -centrality based on estimated network for both datasets (human gut and soil) to identify keystone genus. Figure 10 shows on the y-axis the ranking of genus based on the point estimation of the grand mean (μ), i.e. the log relative abundances. That is, genus on the top correspond to the most abundant microbes (*Clostridium* for human gut and *Terrimonas* for soil). On the x-axis, we show the estimated α -centrality for each genus. For the human gut data, the genus with the highest α -centrality is *Bacteroides* which is an abundant genus and known to have the ability to moderate the host's immune response (Blander et al., 2017) and transfer antibiotic genes to other members of the community (Shoemaker et al., 2001). For the soil data, the genus with highest α -centrality is *Nitrososphaera*. Members of this genus have the ability to perform ammonia oxidizing which might play a major role in nitrification (Tourna et al., 2011) which is crucial in the soil microbial community. We observe a general trend that abundant genus have higher α -centrality, but this trend is not definite. For instance, neither *Bacteroides* nor *Nitrososphaera* have the highest α -centrality estimate. The Spearman correlation coefficients between estimated relative abundance and α -centrality in the human gut dataset is 0.68 while it is 0.58 in the soil dataset. Variation of α -centrality measure is also larger in soil (standard deviation is 0.67 times the mean in the soil data while the standard deviation is 0.38 times the mean in the human gut data). The difference might due to the more variate environmental condition in soil making it difficult to have just one genus taking the central role.

5 Discussion

5.1 Importance of conditional dependence

It is crucial for any model dealing with predictors and multivariate responses to distinguish between marginal effects and conditional effects. A conditional construction coincides with the intuition that the marginal response of a node *should* be influenced by both its and others' reaction to a common input. This distinction of marginal or conditional effects is particularly important when including biological prior knowledge. For example, species reactions to treatments can be measured under controlled experiments (e.g. Lo and Marculescu (2017)) and this knowledge would be properly encoded under a conditional dependence model. See more in the "Agreement with experimenter's intuition on mean behavior" and "Optimal model-based design of experiments" below.

5.2 Flexibility of the Bayesian model

Compared with the frequentist method, the Bayesian method allows an easier extension of the core Normal model to different types of responses via hierarchical structures. As long as one can sample from the full conditional distribution of the (latent) Normal variable, the posterior sampling is a straight-forward extension of the proposed Gibbs sampler. Though not shown here, other commonly encountered models in biology are also simple extensions of our model, e.g. zero-inflated Poisson and multinomial (Lambert, 1992). By using the Normal distribution as the core model, we can automatically take into account the over-dispersion because the model considers the variance parameters explicitly. Note that one common complaint on the LASSO prior is that it does not put any mass on 0 for any edge. Though a spike-and-slab prior is possible, an efficient posterior sampling algorithm like the block Gibbs sampler presented in this work (also in Wang (2012)) would be hard to derive due the intractable normalizing constant.

5.3 Challenges in learning the graphical structure

Graphical selection can be difficult because of the confounding in its own structure. For example, recall Figure 1 A and B. These two graphs can produce a similar correlation between Y_1 and Y_2 . One extreme example is when all links in A and B have no noise (e.g. $Y_1 = X$, $Y_2 = -Y_1$ versus $Y_1 = X$, $Y_2 = -X$). In this extreme example, it is impossible to distinguish graph A from B. Of particular difficulty are also cases like Figure 1 E where all partial correlations are positive (or negative). Additionally, when Ω has bad condition numbers, then \mathbf{B} might have large error in estimation since the marginal mean response and Ω inform the estimation of \mathbf{B} , and a small change in the marginal mean response can have a large influence in \mathbf{B} . Future work could focus on how to use experiments to decouple the confounding of Ω and \mathbf{B} to address some of these challenges.

5.4 Agreement with the experimenter’s intuition on mean behavior

Intuitively, an experimenter should be able to make inferences about the interactions among responses from the behavior of the mean structures under treatment. For example, in Figure 1 D, an experimenter might knock out a gene as the treatment ($X = 1$ for knock out and $X = 0$ for not) and compare the gene expression levels of another gene (Y_2) via a t test. The result of this t test will provide information regarding the interaction between Y_1 and Y_2 because there are no other factors affecting Y_1 and Y_2 is conditionally independent with X . Thus, this experiment is specific to Y_1 and provides information on partial correlation between Y_1 and Y_2 by only affecting Y_1 . That is, any change in Y_2 is due to the partial correlation with Y_1 rather than a reaction to X . It is precisely the fact that the mean of Y_2 in this experiment depends on the correlation between Y_1 and Y_2 that allows experimenters to test differences in means of Y_2 under the effect of the treatment (X) through standard t tests. However, this intuition is violated under the standard linear regression setting. The vector (Y_1, Y_2) is Normally distributed with mean $\mu = (X\beta_1, 0)$ and covariance Σ under the network in Figure 1 D, and thus, the mean of Y_2 is always 0 regardless of the value of X . In contrast, in the CAR parametrization, the mean vector is $\Sigma\mu$ whose second entry is given by $\rho\beta_1X$, i.e. the mean value of Y_2 depends on β_1 (the reaction of Y_1 to the treatment) as well as ρ (the correlation between Y_1 and Y_2). Given that the experimenter’s intuition on specificity is based on the notion of *conditional (in)dependence* between X and Y_1, Y_2 , we conclude that it is desirable that the mean vector contains information on the correlation structure among responses and this is a characteristic of the CAR model that we propose.

5.5 Optimal model-based design of experiments

An experimenter should be able to design experiments that decode the links among response nodes when specific experimental interventions towards one node are possible. In practice, when possible, experimenters will always prefer experiments with better specificity. However, this preference is not evident in the linear regression setting since the Fisher information matrix of the mean vector and the precision matrix is block-diagonal (Malagò and Pistone, 2015), and thus, any information that we have on \mathbf{B} will not affect estimation of Σ . In addition, the information of Σ is not a function of design (\mathbf{X}) no matter whether we have prior knowledge about effect of such experiment (prior on \mathbf{B}). The CAR parametrization avoids this disagreement because the Fisher information matrix is no longer block-diagonal and prior information about the treatment can flow into the estimation of Σ via an optimal model-based experimental design (Chaloner and Verdinelli, 1995). We highlight that due to the confounding between the treatment effect and the interaction among responses, the prior knowledge on specificity of the treatment is necessary for such an optimal model-based experimental design. Future work could investigate the method of experimental design to best decode such networks and the theoretical properties of such designs.

6 Open-source software

We developed our algorithm in R 3.6.3 (R Core Team, 2020) and all the code as well as data used is available as an R package CARLasso hosted on <https://github.com/YunyiShen/CAR-LASSO>. All simulations and data analyses code are in the dev branch of the same repository.

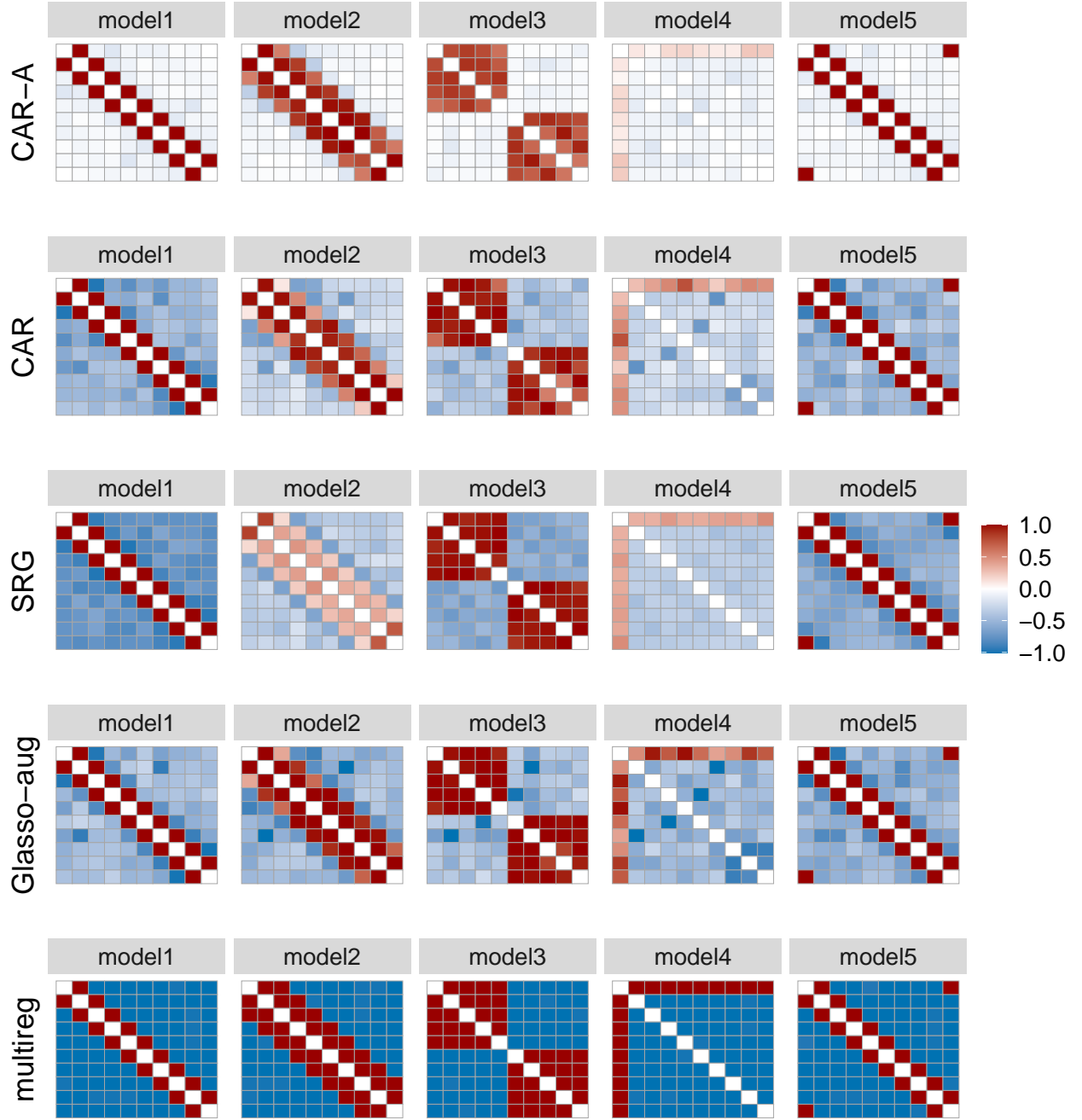


Figure 3: Reconstruction accuracy of the graph among responses (Ω) for $k = 10$ nodes, $p = 10$ predictors and sparsity of 0.8. Red entries correspond to true positive edges and blue entries correspond to false positive edges. Darker color means higher frequency of being estimated in 50 reconstructions. Our proposed method Adaptive CAR-LASSO (CAR-A) outperforms the other methods by displaying the lowest false positive rate (less blue).

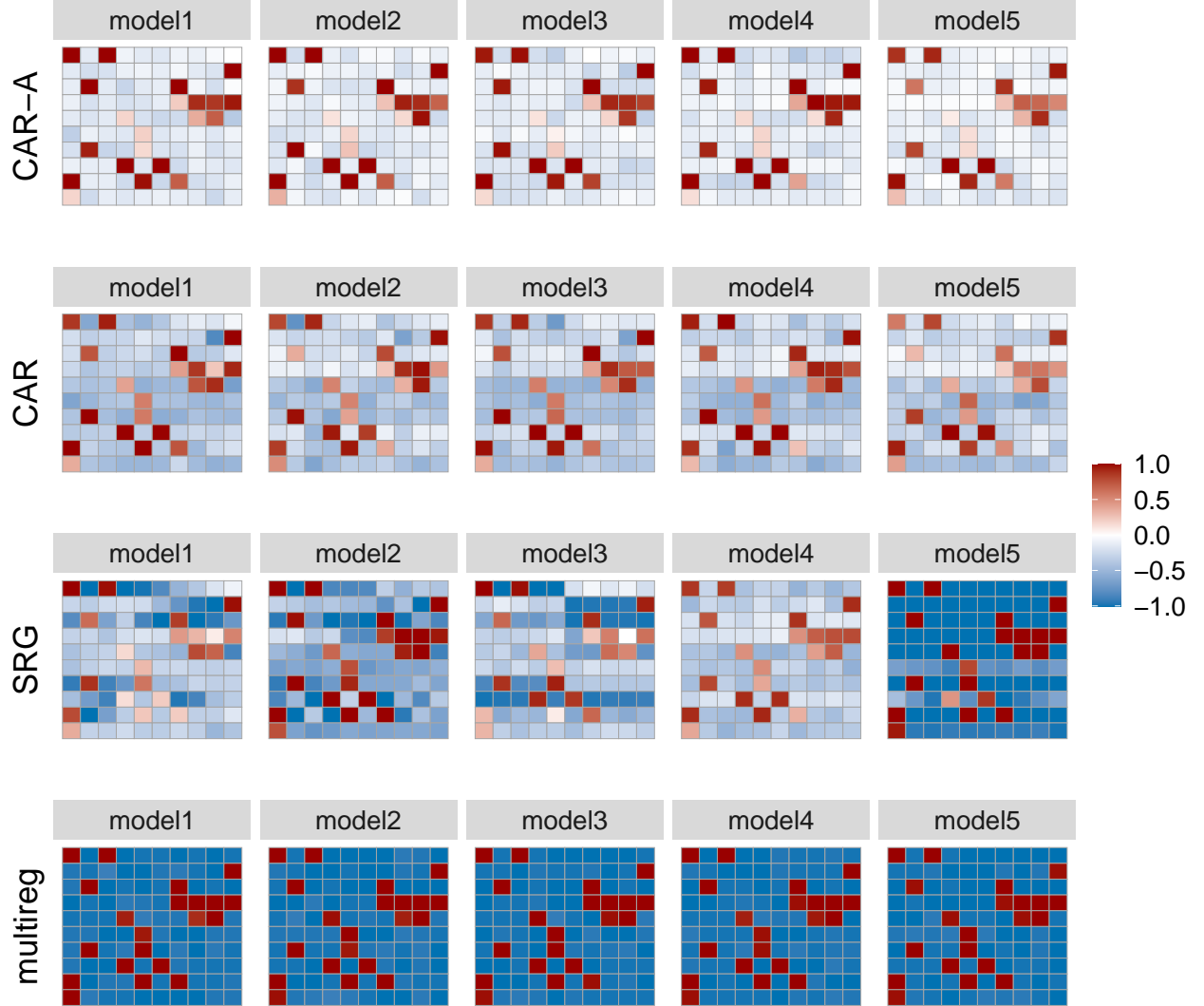


Figure 4: Reconstruction accuracy of the graph between responses and predictors (\mathbf{B}) for $k = 10$ nodes, $p = 10$ predictors and sparsity of 0.8. Red entries correspond to true positive edges and blue entries correspond to false positive edges. Darker color means higher frequency of being estimated in 50 reconstructions. Our proposed method Adaptive CAR-LASSO (CAR-A) outperforms the other methods by displaying the lowest false positive rate (less blue).

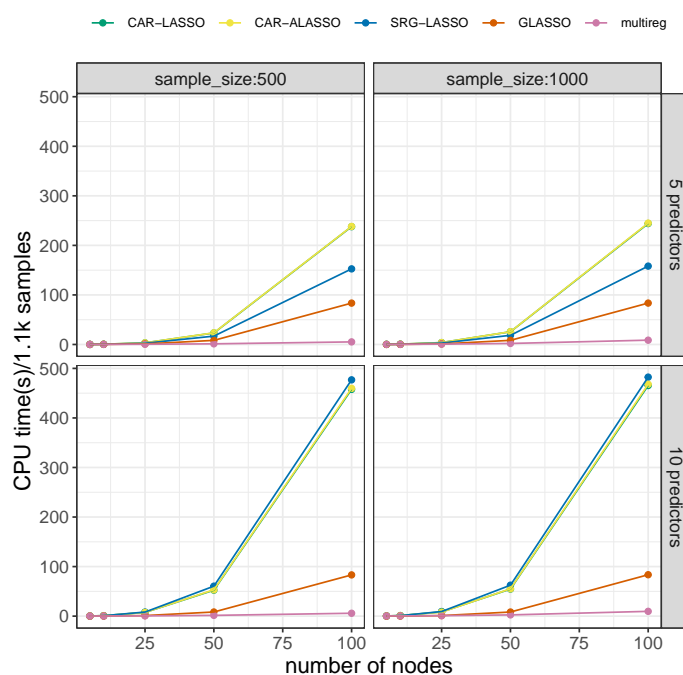


Figure 5: **Scalability test.** Computational time for each algorithm in CPU seconds as a function of the number of nodes, the number of predictors, and sample size. Speed depends on the number of nodes and number of predictors, but not on sample size. Our proposed method is efficient, yet slower than Graphical LASSO

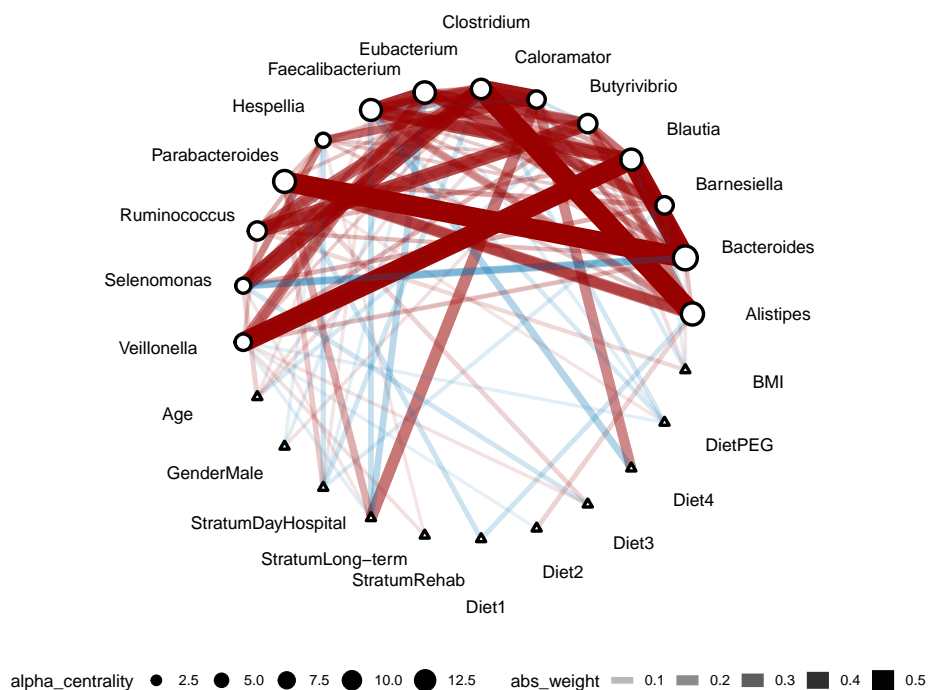


Figure 6: **Reconstructed genus conditional network for human gut microbiota using the adaptive CAR-LASSO model.** Triangle nodes correspond to predictors and circle nodes correspond to relative abundances of genus. The node size on the circle nodes correspond to the α -centrality values (Bonacich and Lloyd, 2001). The width of the edges correspond to the absolute weight, and the color to the type of interaction (red positive, blue negative).

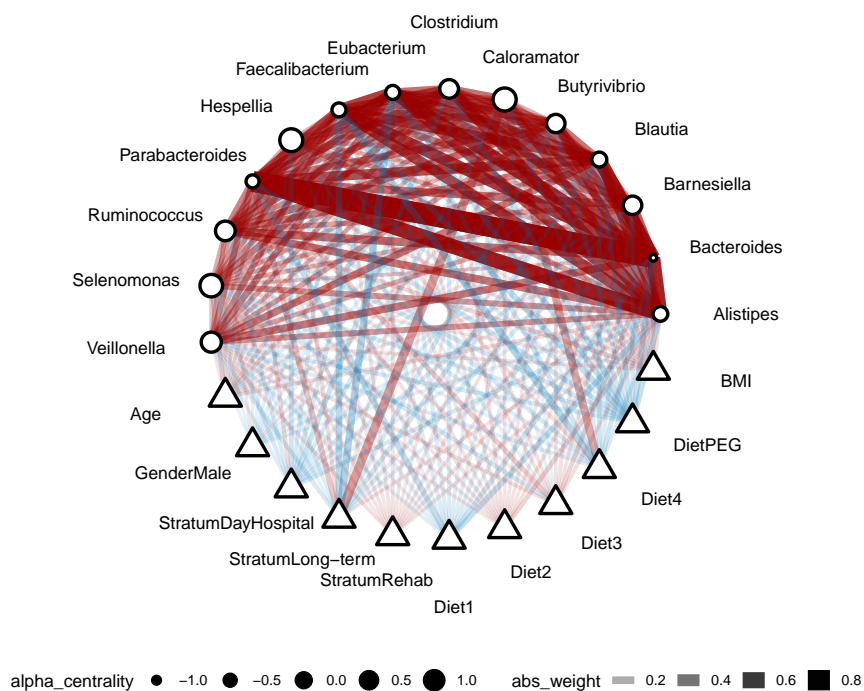


Figure 7: **Reconstructed genus marginal network for human gut microbiota using multiresponse regression.** Triangle nodes correspond to predictors and circle nodes correspond to relative abundances of genus. The node size on the circle nodes correspond to the α -centrality values (Bonacich and Lloyd, 2001). The width of the edges correspond to the absolute weight, and the color to the type of interaction (red positive, blue negative). Edges are marginal rather than conditional. Note that the larger size of the triangles compared to the triangles in the conditional network (Figure 6) are an effect of the shrinkage of the circle nodes in this network.

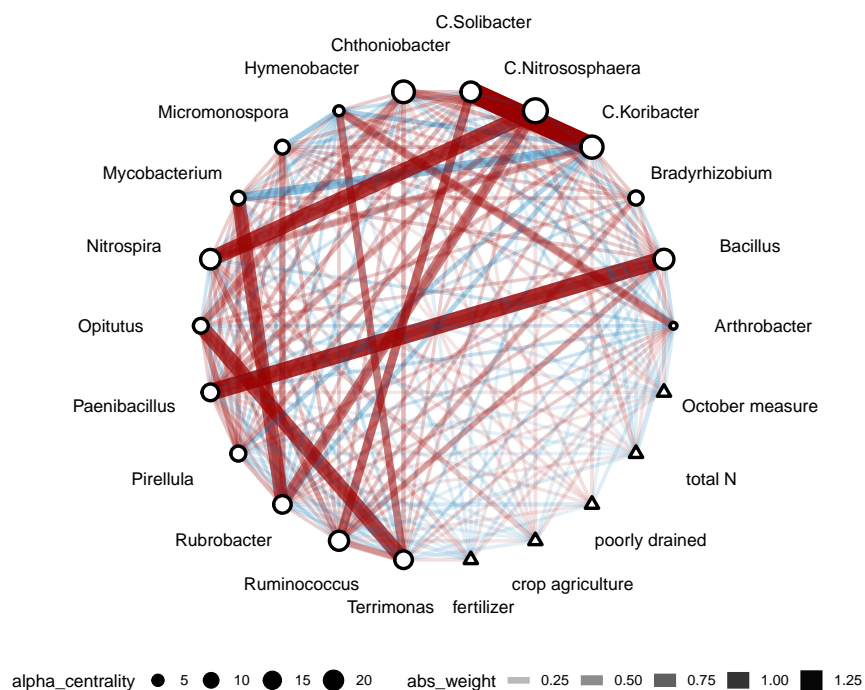


Figure 8: **Reconstructed genus conditional network for soil microbiota using adaptive CAR-LASSO.** Triangle nodes correspond to predictors and circle nodes correspond to relative abundances of genus. The node size on the circle nodes correspond to the α -centrality values (Bonacich and Lloyd, 2001). The width of the edges correspond to the absolute weight, and the color to the type of interaction (red positive, blue negative).

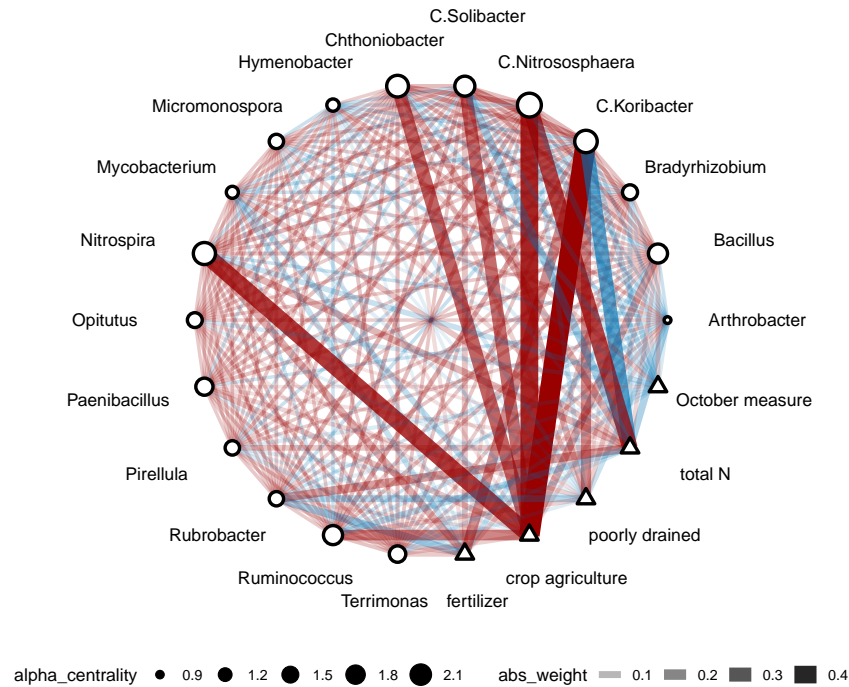


Figure 9: **Reconstructed genus marginal network for soil microbiota using multiresponse regression.** Triangle nodes correspond to predictors and circle nodes correspond to relative abundances of genus. The node size on the circle nodes correspond to the α -centrality values (Bonacich and Lloyd, 2001). The width of the edges correspond to the absolute weight, and the color to the type of interaction (red positive, blue negative). Edges are marginal rather than conditional.

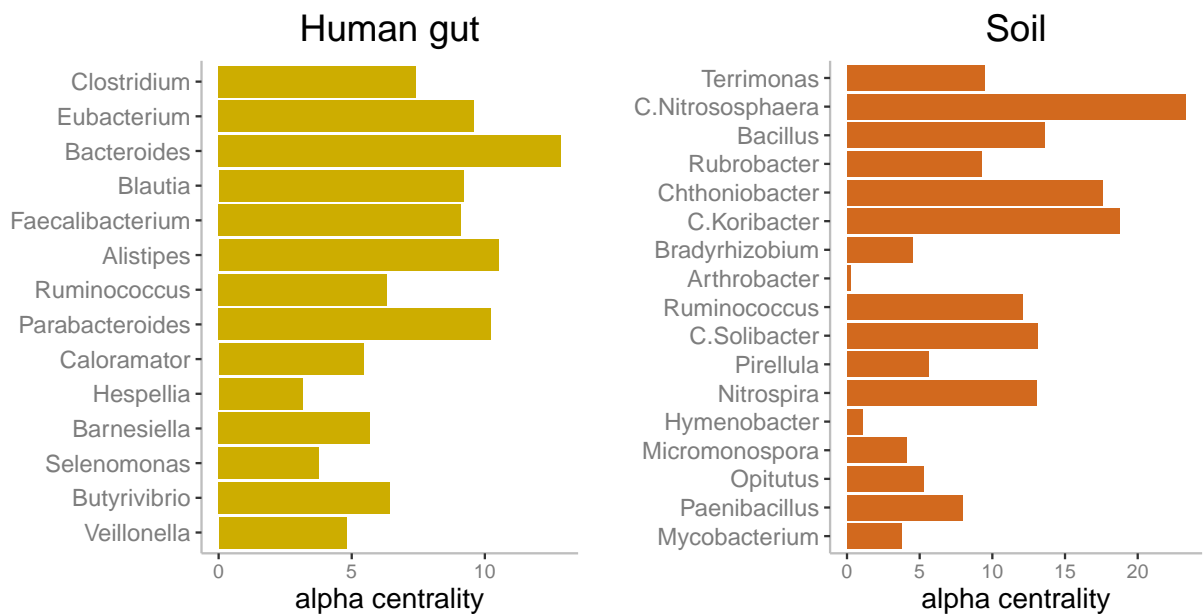


Figure 10: **α -centrality of genus ranked by abundances.** We rank the genus based on estimated relative abundance (upper=higher abundance) and bars correspond to the estimated α -centrality. We see a general trend of abundant genus having higher α -centrality, but it is not definite.

Acknowledgements

This material is based upon work support by the National Institute of Food and Agriculture, United States Department of Agriculture, Hatch project 1023699. This work was also supported by the Department of Energy [DE-SC0021016 to C.S.L.]. Y.S. would like to thank Xiang Li from Peking University for discussion on the Generalized Inverse Gaussian distribution.

References

- Aitchison, J. and Ho, C. H. (1989). The multivariate Poisson-log normal distribution. *Biometrika*, 76(4):643–653.
- Allsup, C. and Lankau, R. (2019). Migration of soil microbes may promote tree seedling tolerance to drying conditions. *Ecology*, 100:e02729.
- Andersson, S. A., Madigan, D., and Perlman, M. D. (2001). Alternative markov properties for chain graphs. *Scandinavian journal of statistics*, 28(1):33–85.
- Andrews, D. F. and Mallows, C. L. (1974). Scale mixtures of normal distributions. *Journal of the Royal Statistical Society: Series B (Methodological)*, 36(1):99–102.
- Bach, E. M., Williams, R. J., Hargreaves, S. K., Yang, F., and Hofmockel, K. S. (2018). Greatest soil microbial diversity found in micro-habitats. *Soil biology and Biochemistry*, 118:217–226.
- Blanchet, F. G., Cazelles, K., and Gravel, D. (2020). Co-occurrence is not evidence of ecological interactions. *Ecology Letters*.
- Blander, J. M., Longman, R. S., Iliev, I. D., Sonnenberg, G. F., and Artis, D. (2017). Regulation of inflammation by microbiota interactions with the host. *Nature immunology*, 18(8):851–860.
- Bonacich, P. and Lloyd, P. (2001). Eigenvector-like measures of centrality for asymmetric relations. *Social networks*, 23(3):191–201.
- Carvalho, C. M., Polson, N. G., and Scott, J. G. (2010). The horseshoe estimator for sparse signals. *Biometrika*, 97(2):465–480.
- Cates, A. M., Braus, M. J., Whitman, T. L., and Jackson, R. D. (2019). Separate drivers for microbial carbon mineralization and physical protection of carbon. *Soil Biology and Biochemistry*, 133:72–82.
- Chaloner, K. and Verdinelli, I. (1995). Bayesian experimental design: A review. *Statistical Science*, pages 273–304.
- Claesson, M. J., Jeffery, I. B., Conde, S., Power, S. E., O’connor, E. M., Cusack, S., Harris, H. M., Coakley, M., Lakshminarayanan, B., O’Sullivan, O., et al. (2012). Gut microbiota composition correlates with diet and health in the elderly. *Nature*, 488(7410):178–184.
- Dave, M., Higgins, P. D., Middha, S., and Rioux, K. P. (2012). The human gut microbiome: current knowledge, challenges, and future directions. *Translational Research*, 160(4):246 – 257. In-Depth Review: Of Microbes and Men: Challenges of the Human Microbiome.
- Fan, J., Feng, Y., and Wu, Y. (2009). Network exploration via the adaptive lasso and scad penalties. *The annals of applied statistics*, 3(2):521.
- Fierer, N., Lauber, C. L., Ramirez, K. S., Zaneveld, J., Bradford, M. A., and Knight, R. (2012). Comparative metagenomic, phylogenetic and physiological analyses of soil microbial communities across nitrogen gradients. *The ISME Journal*, 6(5):1007–1017.
- Friedman, J., Hastie, T., and Tibshirani, R. (2008). Sparse inverse covariance estimation with the graphical lasso. *Biostatistics*, 9(3):432–441.
- Frydenberg, M. (1990). The chain graph markov property. *Scandinavian Journal of Statistics*, pages 333–353.
- Gilks, W. R. and Wild, P. (1992). Adaptive rejection sampling for gibbs sampling. *Journal of the Royal Statistical Society: Series C (Applied Statistics)*, 41(2):337–348.
- Hofmockel, K. (2012). Hofmockel soil aggregate cob kbase (mgp2592). <https://www.mg-rast.org/mgmain.html?mgpage=project&project=mgp2592>.
- Hörmann, W. and Leydold, J. (2014). Generating generalized inverse gaussian random variates. *Statistics and Computing*, 24(4):547–557.
- Jones, B., Carvalho, C., Dobra, A., Hans, C., Carter, C., and West, M. (2005). Experiments in stochastic computation for high-dimensional graphical models. *Statistical Science*, pages 388–400.

- Jorgensen, B. (2012). *Statistical properties of the generalized inverse Gaussian distribution*, volume 9. Springer Science and Business Media.
- Kranz, C. and Whitman, T. (2019). Short communication: Surface charring from prescribed burning has minimal effects on soil bacterial community composition two weeks post-fire in jack pine barrens. *Applied Soil Ecology*, 144:134–138.
- Lambert, D. (1992). Zero-inflated poisson regression, with an application to defects in manufacturing. *Technometrics*, 34(1):1–14.
- Lankau, E. W., Xue, D., Chrisensen, R., Gevens, A. J., and Lankau, R. A. (2020a). Management and soil conditions influence common scab severity on potato tubers via indirect effects on soil microbial communities. *Phytopathology*TM.
- Lankau, R., George, I., and Miao, M. (2020b). Crop health optimized by microbial diversity across phylogenetic scales. *Submitted*.
- Lauritzen, S. L. and Richardson, T. S. (2002). Chain graph models and their causal interpretations. *Journal of the Royal Statistical Society: Series B (Statistical Methodology)*, 64(3):321–348.
- Lauritzen, S. L. and Wermuth, N. (1989). Graphical models for associations between variables, some of which are qualitative and some quantitative. *The annals of Statistics*, pages 31–57.
- Leng, C., Tran, M. N., and Nott, D. (2014). Bayesian adaptive Lasso. *Annals of the Institute of Statistical Mathematics*, 66(2):221–244.
- Lo, C. and Marculescu, R. (2017). Mplasso: Inferring microbial association networks using prior microbial knowledge. *PLoS computational biology*, 13(12):e1005915.
- Malagò, L. and Pistone, G. (2015). Information geometry of the gaussian distribution in view of stochastic optimization. In *Proceedings of the 2015 ACM Conference on Foundations of Genetic Algorithms XIII*, pages 150–162.
- Meyer, F., Paarmann, D., D’Souza, M., Olson, R., Glass, E. M., Kubal, M., Paczian, T., Rodriguez, A., Stevens, R., Wilke, A., et al. (2008). The metagenomics rast server—a public resource for the automatic phylogenetic and functional analysis of metagenomes. *BMC bioinformatics*, 9(1):1–8.
- O’Toole, P. W. (2008). Gut microbiota in the irish elderly and its links to health and diet (mgp154). <https://www.mg-rast.org/mgmain.html?mgpage=project&project=mgp154>.
- Park, T. and Casella, G. (2008). The Bayesian Lasso. *Journal of the American Statistical Association*, 103(482):681–686.
- R Core Team (2020). *R: A Language and Environment for Statistical Computing*. R Foundation for Statistical Computing, Vienna, Austria.
- Rioux, R. A., Stephens, C. M., and Kerns, J. P. (2019). Factors affecting pathogenicity of the turfgrass dollar spot pathogen in natural and model hosts. *bioRxiv*, page 630582.
- Shoemaker, N., Vlamakis, H., Hayes, K., and Salyers, A. (2001). Evidence for extensive resistance gene transfer among bacteroides spp. and among bacteroides and other genera in the human colon. *Applied and environmental microbiology*, 67(2):561–568.
- Tourna, M., Stieglmeier, M., Spang, A., Könneke, M., Schintlmeister, A., Urich, T., Engel, M., Schlöter, M., Wagner, M., Richter, A., et al. (2011). Nitrososphaera viennensis, an ammonia oxidizing archaeon from soil. *Proceedings of the National Academy of Sciences*, 108(20):8420–8425.
- Turnbaugh, P. J., Ley, R. E., Hamady, M., Fraser-Liggett, C. M., Knight, R., and Gordon, J. I. (2007). The human microbiome project. *Nature*, 449(7164):804–810.
- Ver Hoef, J. M., Hanks, E. M., and Hooten, M. B. (2018). On the relationship between conditional (CAR) and simultaneous (SAR) autoregressive models. *Spatial Statistics*, 25:68–85.
- Wang, H. (2012). Bayesian graphical lasso models and efficient posterior computation. *Bayesian Analysis*, 7(4):867–886.
- Whitman, T., Neurath, R., Perera, A., Chu-Jacoby, I., Ning, D., Zhou, J., Nico, P., Pett-Ridge, J., and Firestone, M. (2018). Microbial community assembly differs across minerals in a rhizosphere microcosm. *Environmental Microbiology*, 20(12):4444–4460.
- Whitman, T., Whitman, E., Woolet, J., Flannigan, M. D., Thompson, D. K., and Parisien, M.-A. (2019). Soil bacterial and fungal response to wildfires in the canadian boreal forest across a burn severity gradient. *Soil Biology and Biochemistry*, 138:107571.
- Xia, F., Chen, J., Fung, W. K., and Li, H. (2013). A logistic normal multinomial regression model for microbiome compositional data analysis. *Biometrics*, 69(4):1053–1063.
- Xie, S., Zeng, D., and Wang, Y. (2021). Integrative network learning for multimodality biomarker data. *The Annals of Applied Statistics*, 15(1):64 – 87.

A Derivation of the Gibbs sampling

Let $\mathbf{1}_n$ be the column vector of ones with dimension n , let $\mathbf{S} = \mathbf{Y}^T \mathbf{Y} \in \mathbb{R}^{k \times k}$ (here we have samples as row vectors in \mathbf{Y}), let $\hat{\mu} = \mathbf{X}\mathbf{B} + \mathbf{1}_n \mu^T$, and let $\mathbf{U} = \hat{\mu}^T \hat{\mu} \in \mathbb{R}^{k \times k}$. Equation A1 shows the full conditional distribution of Ω and η (the hyperparameters in Equation 2).

$$p(\Omega, \eta | \mathbf{Y}, \lambda_\Omega, \hat{\mu}) \propto |\Omega|^{\frac{n}{2}} \exp\left(-\frac{1}{2} \text{tr}(\mathbf{S}\Omega) - \frac{1}{2} \text{tr}(\mathbf{U}\Omega^{-1})\right) \prod_{m < l} \left[\frac{1}{\sqrt{2\pi\eta_{ml}}} \exp\left(-\frac{\omega_{ml}^2}{2\eta_{ml}}\right) \right] \\ \times \prod_{m=1}^k \left[\frac{\lambda_\Omega}{2} \exp\left(-\frac{\lambda_\Omega \omega_{mm}}{2}\right) \right] I_{\Omega \in M^+} \quad (\text{A1})$$

We can update one row (column) at one iteration. Let \mathbf{H} be the symmetric matrix with $\mathbf{H}_{ml} = \mathbf{H}_{lm} = \eta_{ml}$ ($m < l$) on the off-diagonal entries and on the diagonal $\mathbf{H}_{mm} = 0$. We take one column out and partition Ω , \mathbf{S} , \mathbf{U} , and \mathbf{H} . Without lose of generality, we show the sampling scheme for the last row (column). Let $\Omega_{11} \in \mathbb{R}^{(k-1) \times (k-1)}$, $\omega_{12} \in \mathbb{R}^{k-1}$, and $\omega_{22} \in \mathbb{R}$. We partition \mathbf{S} , \mathbf{U} and \mathbf{H} in the same manner.

$$\Omega = \begin{bmatrix} \Omega_{11} & \omega_{12} \\ \omega_{12}^T & \omega_{22} \end{bmatrix}, \mathbf{S} = \begin{bmatrix} \mathbf{S}_{11} & s_{12} \\ s_{12}^T & s_{22} \end{bmatrix}, \mathbf{U} = \begin{bmatrix} \mathbf{U}_{11} & \mathbf{u}_{12} \\ \mathbf{u}_{12}^T & u_{22} \end{bmatrix}, \mathbf{H} = \begin{bmatrix} \mathbf{H}_{11} & \eta_{12} \\ \eta_{12}^T & 0 \end{bmatrix}.$$

By setting

$$\gamma = \omega_{22} - \omega_{12}^T \Omega_{11}^{-1} \omega_{12} \in \mathbb{R}, \quad (\text{A2})$$

Ω^{-1} can be written in a block form:

$$\Omega^{-1} = \begin{bmatrix} \Omega_{11}^{-1} + \frac{1}{\gamma} \Omega_{11}^{-1} \omega_{12} \omega_{12}^T \Omega_{11}^{-1} & -\frac{1}{\gamma} \Omega_{11}^{-1} \omega_{12} \\ -\frac{1}{\gamma} \omega_{12}^T \Omega_{11}^{-1} & \frac{1}{\gamma} \end{bmatrix}.$$

Given

$$\text{tr}(\mathbf{U}\Omega^{-1}) = \text{tr}(\mathbf{U}_{11}\Omega_{11}^{-1}) + \frac{1}{\gamma} (\omega_{12}^T \Omega_{11}^{-1} \mathbf{U}_{11} \Omega_{11}^{-1} \omega_{12} - 2\mathbf{u}_{12}^T \Omega_{11}^{-1} \omega_{12} + u_{22}),$$

we have the full conditional distribution of ω_{12} and γ :

$$p(\omega_{12}, \gamma | \Omega_{11}, \eta, \lambda_\Omega) \propto \gamma^{\frac{n}{2}} \exp\left(-\frac{1}{2}(s_{22} + \lambda_\Omega)\gamma - \frac{u_{22}}{2\gamma}\right) \\ \times \exp\left\{-\left[s_{12} - \frac{1}{\gamma} \Omega_{11}^{-1} \mathbf{u}_{12}\right]^T \omega_{12} - \frac{1}{2} \omega_{12}^T [D_\eta^{-1} + (s_{22} + \lambda_\Omega) \Omega_{11}^{-1} + \frac{1}{\gamma} \Omega_{11}^{-1} \mathbf{U}_{11} \Omega_{11}^{-1}] \omega_{12}\right\}.$$

From the above equation, we get a closed form expression for the conditional distribution of γ :

$$p(\gamma | \omega_{12}, \Omega_{11}, \eta, \lambda_\Omega) \propto \gamma^{\frac{n}{2}} \exp\left(-\frac{1}{2}(s_{22} + \lambda_\Omega)\gamma - \frac{u_{22} - 2\mathbf{u}_{12}^T \Omega_{11}^{-1} \omega_{12} + \omega_{12}^T \Omega_{11}^{-1} \mathbf{U}_{11} \Omega_{11}^{-1} \omega_{12}}{2\gamma}\right) I_{\gamma \geq 0} \quad (\text{A3})$$

which is a Generalized Inverse Gaussian (GIG) distribution (Hörmann and Leydold, 2014; Jorgensen, 2012) with parameters:

$$\lambda = \frac{n}{2} + 1 \\ \psi = s_{22} + \lambda_\Omega \\ \chi = u_{22} - 2\mathbf{u}_{12}^T \Omega_{11}^{-1} \omega_{12} + \omega_{12}^T \Omega_{11}^{-1} \mathbf{U}_{11} \Omega_{11}^{-1} \omega_{12}.$$

GIG has a positive support. Thus, the determinant and the k^{th} principal minor of the updated Ω are positive, while the first $k - 1$ principal minors remain unchanged and positive. In this manner, the updated Ω always remains positive definite.

By denoting $\mathbf{D}_\eta = \text{diag}(\boldsymbol{\eta}_{12}) \in \mathbb{R}^{(k-1) \times (k-1)}$, the full conditional distribution of $\boldsymbol{\omega}_{12}$ is a Normal distribution:

$$p(\boldsymbol{\omega}_{12} | \gamma, \boldsymbol{\Omega}_{11}, \eta, \lambda_\Omega) \propto \exp\left\{-\left[\mathbf{s}_{12} - \frac{1}{\gamma} \boldsymbol{\Omega}_{11}^{-1} \mathbf{u}_{12}\right]^T \boldsymbol{\omega}_{12} - \frac{1}{2} \boldsymbol{\omega}_{12}^T [\mathbf{D}_\eta^{-1} + (s_{22} + \lambda_\Omega) \boldsymbol{\Omega}_{11}^{-1} + \frac{1}{\gamma} \boldsymbol{\Omega}_{11}^{-1} \mathbf{U}_{11} \boldsymbol{\Omega}_{11}^{-1}] \boldsymbol{\omega}_{12}\right\} \quad (\text{A4})$$

with parameters:

$$\begin{aligned} \boldsymbol{\Sigma}_{\boldsymbol{\omega}_{12}}^{-1} &= \mathbf{D}_\eta^{-1} + (s_{22} + \lambda_\Omega) \boldsymbol{\Omega}_{11}^{-1} + \frac{1}{\gamma} \boldsymbol{\Omega}_{11}^{-1} \mathbf{U}_{11} \boldsymbol{\Omega}_{11}^{-1} \\ \boldsymbol{\mu}_{\boldsymbol{\omega}_{12}} &= -\boldsymbol{\Sigma}_{\boldsymbol{\omega}_{12}}^{-1} \left[\mathbf{s}_{12} - \frac{1}{\gamma} \boldsymbol{\Omega}_{11}^{-1} \mathbf{u}_{12} \right]. \end{aligned}$$

As in Wang (2012), the $z_{ij} = 1/\eta_{ij}$ are independent Inverse Gaussians with parameters:

$$\begin{aligned} \mu_{z_{ij}} &= \sqrt{\lambda_\Omega^2 / \omega_{ij}^2} \\ \lambda_{z_{ij}} &= \lambda_\Omega^2 \end{aligned}$$

and density:

$$p(z_{ij} | \boldsymbol{\Omega}, \lambda_\Omega) = \left(\frac{\lambda_{z_{ij}}}{2\pi z_{ij}^3} \right)^{1/2} \exp\left(-\frac{\lambda_{z_{ij}} (z_{ij} - \mu_{z_{ij}})^2}{2(\mu_{z_{ij}})^2 z_{ij}} \right) I_{z_{ij} > 0}. \quad (\text{A5})$$

The full conditional distribution of $\text{vec}(\mathbf{B})$ can be represented using tensor product (Leng et al., 2014). Let $\mathbf{D}_{\tau^2} = \text{diag}(\tau^2) \in \mathbb{R}^{kp \times kp}$ for τ the scaling parameters in the prior density of \mathbf{B} (Equation 2). Then, the conditional distribution of $\text{vec}(\mathbf{B})$ has the following form:

$$\begin{aligned} p(\text{vec}(\mathbf{B}) | \mathbf{D}_{\tau^2}, \boldsymbol{\Omega}, \mu, \mathbf{X}, \mathbf{Y}) &\propto \exp\{\mathbf{X}^T (\mathbf{Y} - \mathbf{1}_n \mu^T \boldsymbol{\Omega}^{-1}) \\ &\quad - \frac{1}{2} \text{vec}(\mathbf{B})^T (\boldsymbol{\Omega}^{-1} \otimes \mathbf{X}^T \mathbf{X} + \mathbf{D}_{\tau^2}^{-1}) \text{vec}(\mathbf{B})\}. \end{aligned} \quad (\text{A6})$$

Note that the information from data is encoded by $\boldsymbol{\Omega}^{-1} \otimes \mathbf{X}^T \mathbf{X}$ which differs from the canonical parameterization of the multiresponse linear regression model in which the information from data is encoded by $\boldsymbol{\Omega} \otimes \mathbf{X}^T \mathbf{X}$. This is because in the kernel of the likelihood, the term involving \mathbf{B} is $\mathbf{X}_i \mathbf{B} \boldsymbol{\Omega}^{-1} \boldsymbol{\Omega} \boldsymbol{\Omega}^{-1} \mathbf{B}^T \mathbf{X}_i^T = \mathbf{X}_i \mathbf{B} \boldsymbol{\Omega}^{-1} \mathbf{B}^T \mathbf{X}_i^T$, instead of $\mathbf{X}_i \tilde{\mathbf{B}} \tilde{\boldsymbol{\Omega}} \tilde{\mathbf{B}}^T \mathbf{X}_i^T$ as in the canonical parametrization (see Section 2.2).

Finally, we update $1/\tau_{ij}$ using an Inverse Gaussian distribution with parameters $\sqrt{\lambda_\beta^2 / \mathbf{B}_{ij}^2}$ and λ_β^2 , and we update μ using a Normal distribution with mean $(\mathbf{Y} \boldsymbol{\Omega} - \mathbf{X} \mathbf{B})^T$ and variance $\boldsymbol{\Omega}/n$.

B Simulation Figures

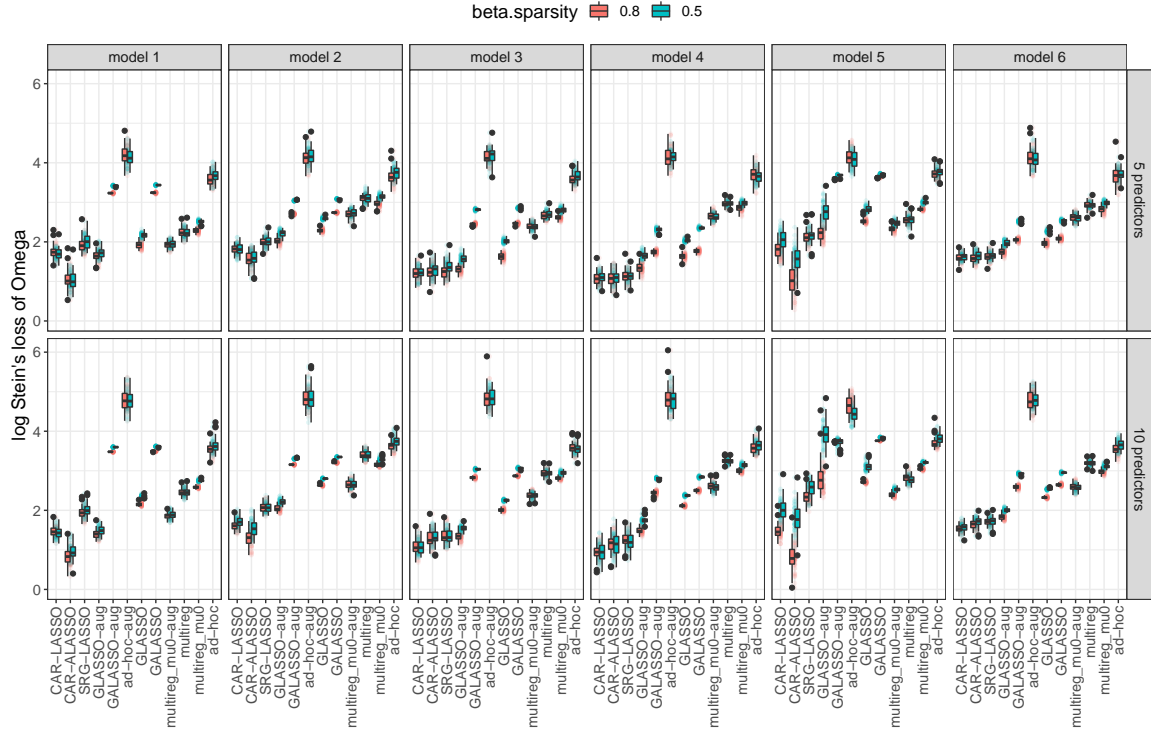


Figure A1: **Stein's Loss of Ω** , (Y-axis in logarithmic scale) for simulated datasets with 30 nodes and 50 samples under two levels of beta sparsity (red 0.8 and blue 0.5), two different number of predictors (10 in bottom row and 5 in top row) and six covariance models (columns). X-axis corresponds to the models compared. Our models (Adaptive) CAR-LASSO get the lowest loss in most cases.

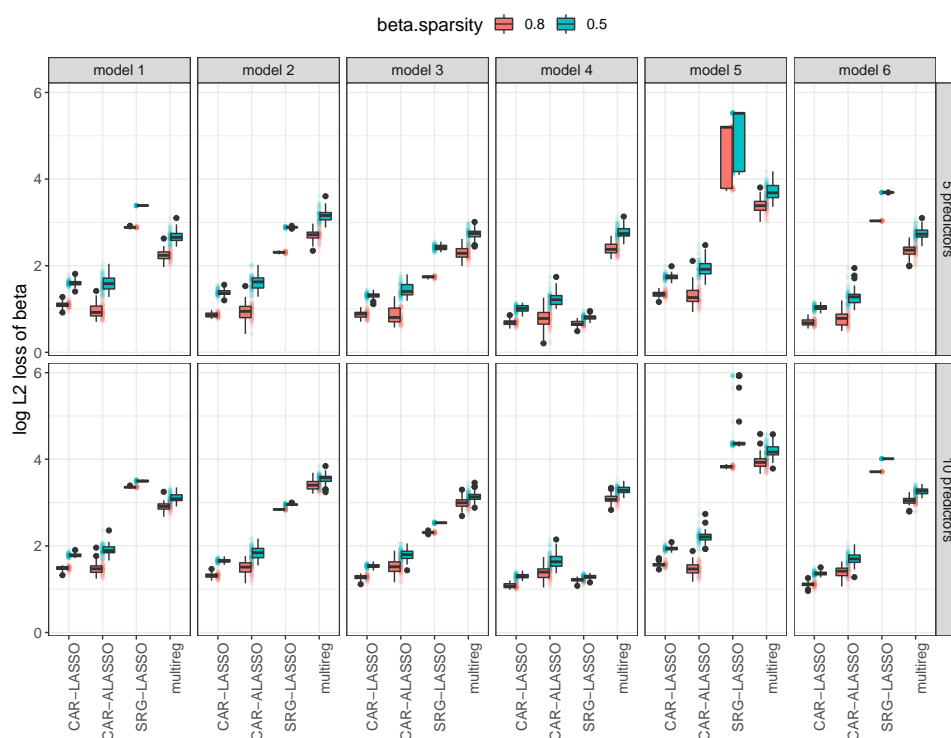


Figure A2: **L2 Loss of β** (Y-axis in logarithmic scale) for simulated datasets with 30 nodes and 50 samples under two levels of beta sparsity (red 0.8 and blue 0.5), two different number of predictors (10 in bottom row and 5 in top row) and six covariance models (columns). X-axis corresponds to the models compared. Our models (Adaptive) CAR-LASSO get the lowest loss in most cases.

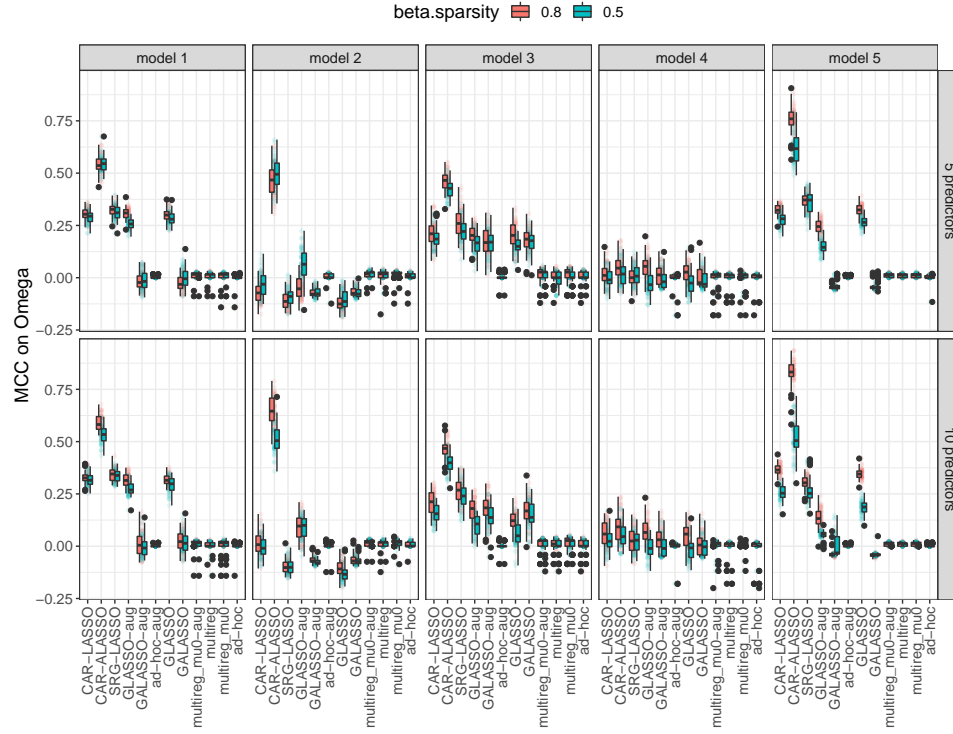


Figure A3: **Matthews Correlation Coefficients for Ω** for simulated datasets with 30 nodes and 50 samples under two levels of beta sparsity (red 0.8 and blue 0.5), two different number of predictors (10 in bottom row and 5 in top row) and six covariance models (columns, fully connected covariance model was omitted from Ω result since MCC was not defined). X-axis corresponds to the models compared. MCC=1 means a perfect reconstruction. Our model Adaptive CAR-LASSO gets the highest MCC in most cases.

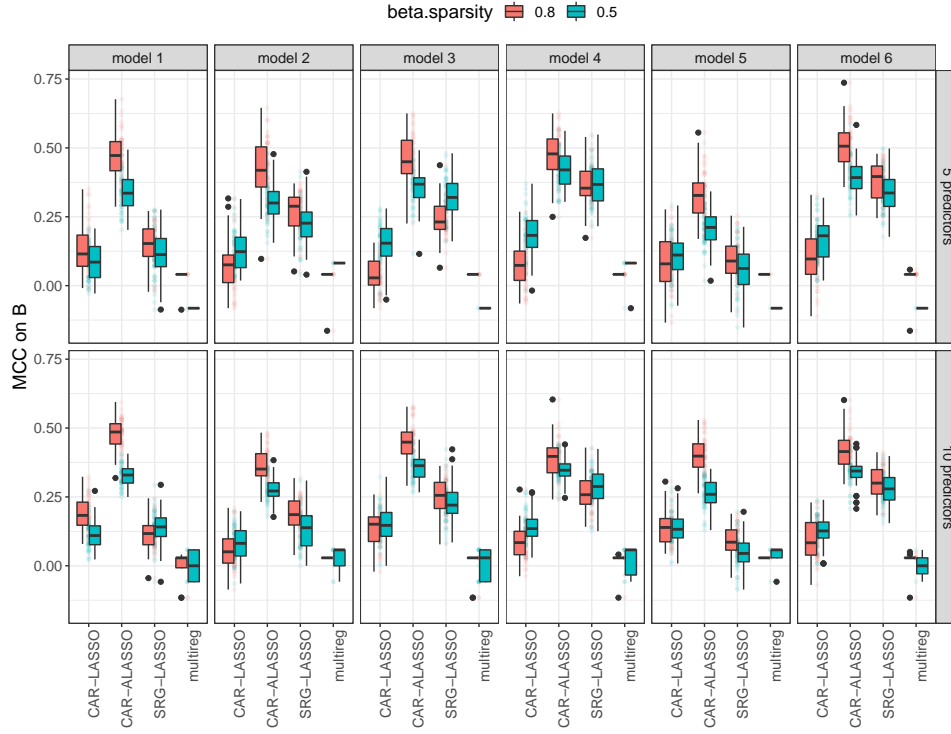


Figure A4: **Matthews Correlation Coefficients for B** for simulated datasets with 30 nodes and 50 samples under two levels of beta sparsity (red 0.8 and blue 0.5), two different number of predictors (10 in bottom row and 5 in top row) and six covariance models (columns, fully connected covariance model was omitted from Ω result since MCC was not defined). X-axis corresponds to the models compared. MCC=1 means a perfect reconstruction. Our model Adaptive CAR-LASSO gets the highest MCC in most cases.

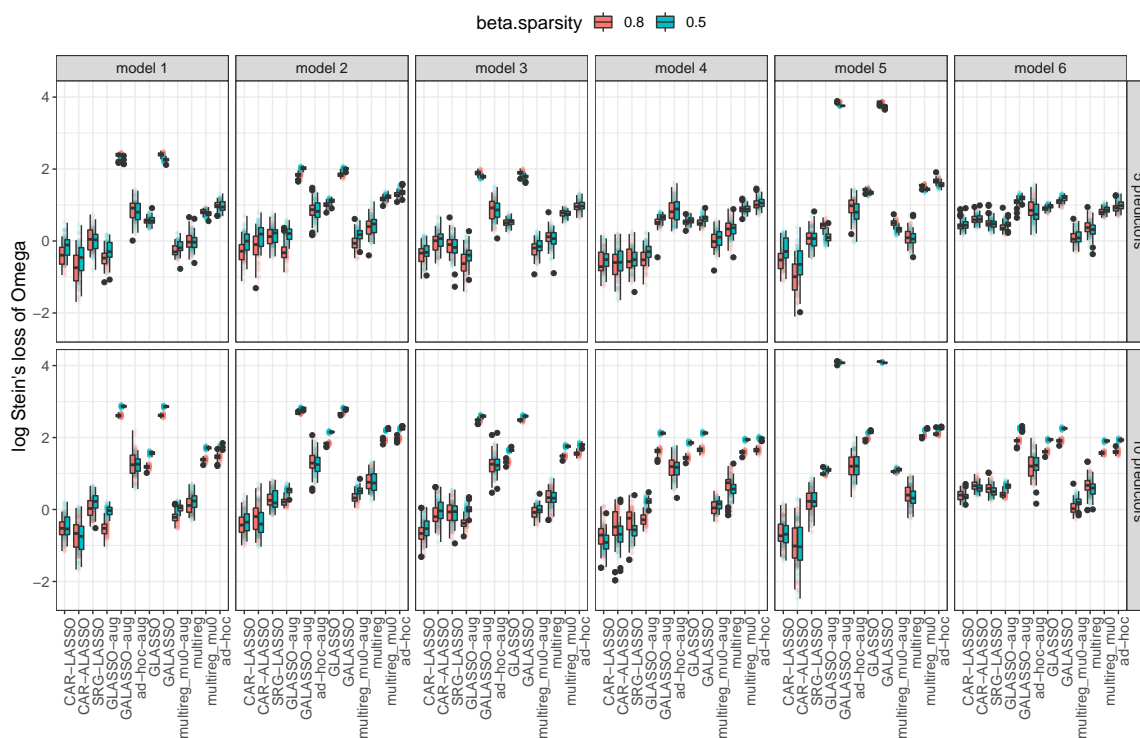


Figure A5: **Stein's Loss of Ω** , (Y-axis in logarithmic scale) for simulated datasets with 10 nodes and 50 samples under two levels of beta sparsity (red 0.8 and blue 0.5), two different number of predictors (10 in bottom row and 5 in top row) and six covariance models (columns). X-axis corresponds to the models compared. Our models (Adaptive) CAR-LASSO get the lowest loss in most cases.

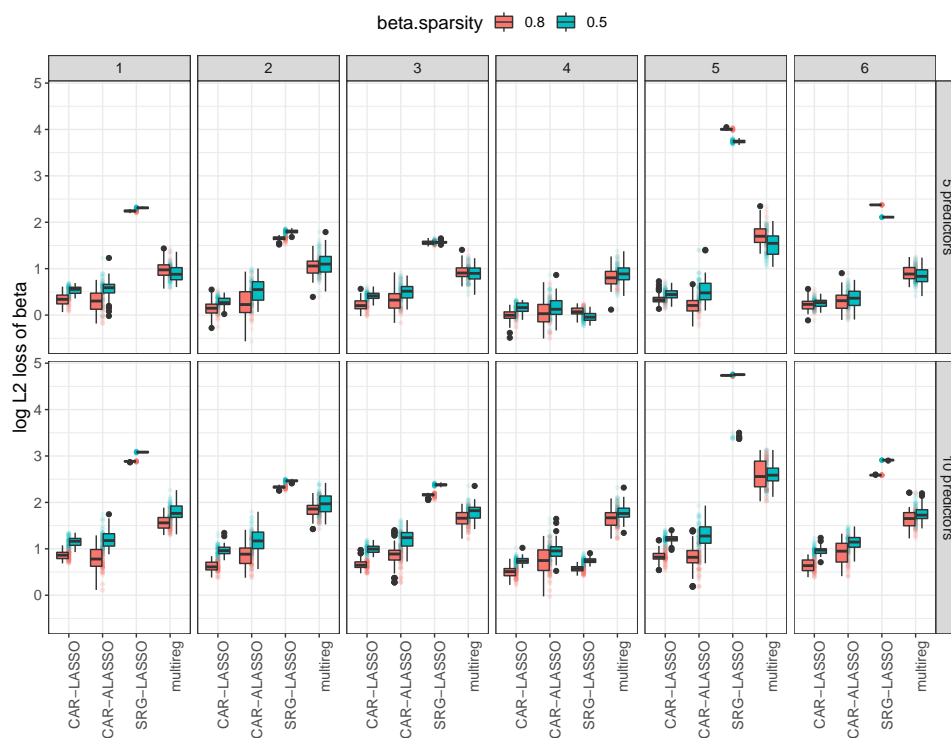


Figure A6: **L2 Loss of β** (Y-axis in logarithmic scale) for simulated datasets with 10 nodes and 50 samples under two levels of beta sparsity (red 0.8 and blue 0.5), two different number of predictors (10 in bottom row and 5 in top row) and six covariance models (columns). X-axis corresponds to the models compared. Our models (Adaptive) CAR-LASSO get the lowest loss in most cases.

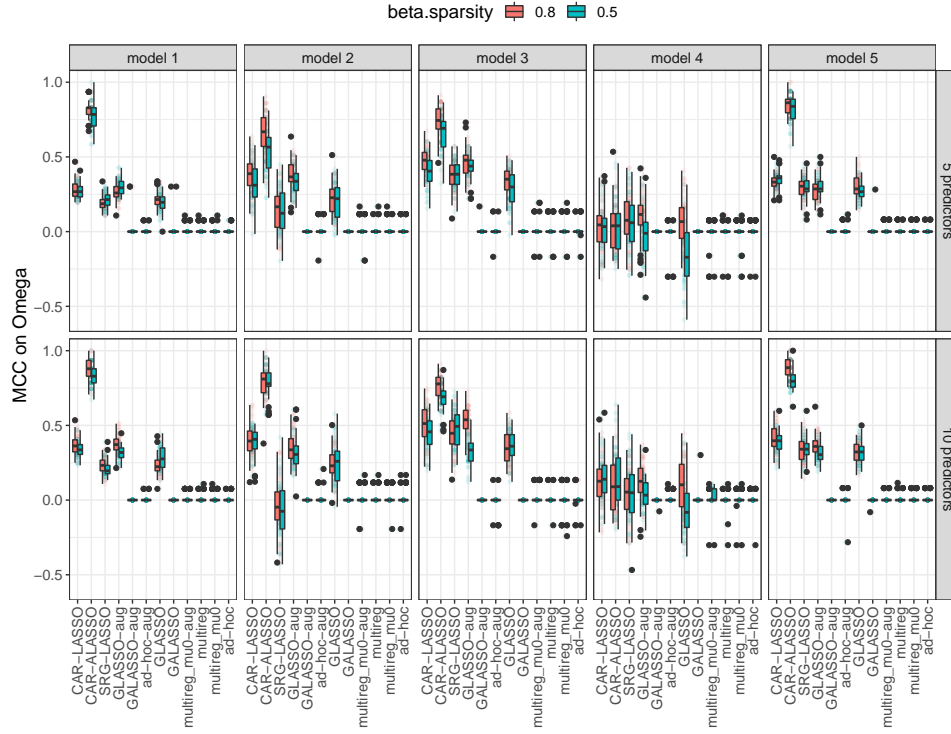


Figure A7: **Matthews Correlation Coefficients for Ω** for simulated datasets with 10 nodes and 50 samples under two levels of beta sparsity (red 0.8 and blue 0.5), two different number of predictors (10 in bottom row and 5 in top row) and six covariance models (columns, fully connected covariance model was omitted from Ω result since MCC was not defined). X-axis corresponds to the models compared. MCC=1 means a perfect reconstruction. Our model Adaptive CAR-LASSO gets the highest MCC in most cases.

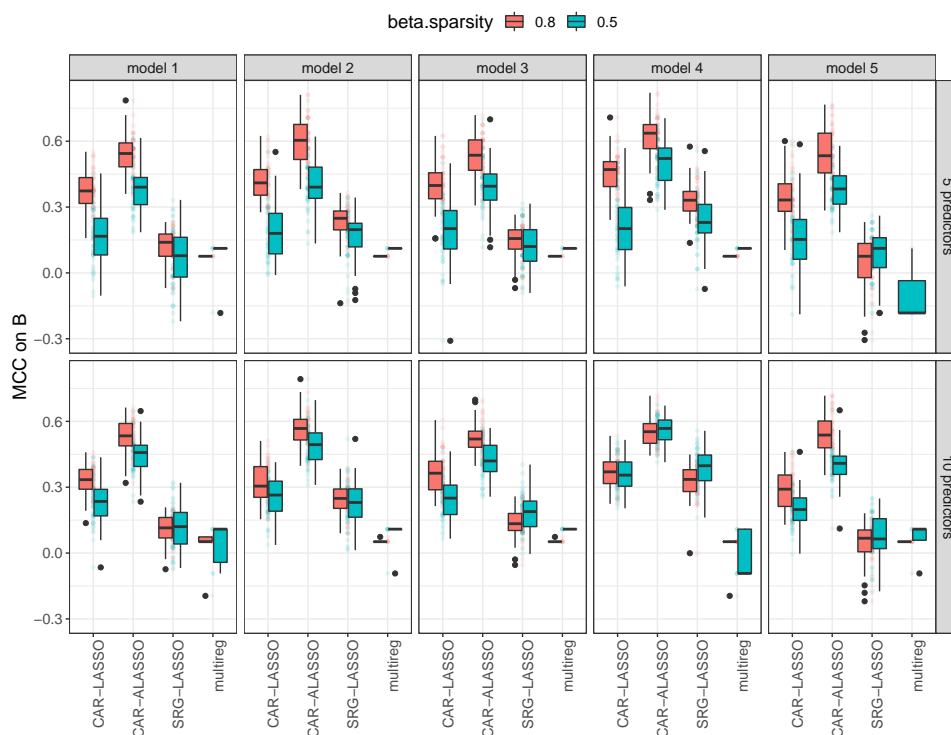


Figure A8: **Matthews Correlation Coefficients for B** for simulated datasets with 10 nodes and 50 samples under two levels of beta sparsity (red 0.8 and blue 0.5), two different number of predictors (10 in bottom row and 5 in top row) and six covariance models (columns, fully connected covariance model was omitted from Ω result since MCC was not defined). X-axis corresponds to the models compared. MCC=1 means a perfect reconstruction. Our model Adaptive CAR-LASSO gets the highest MCC in most cases.

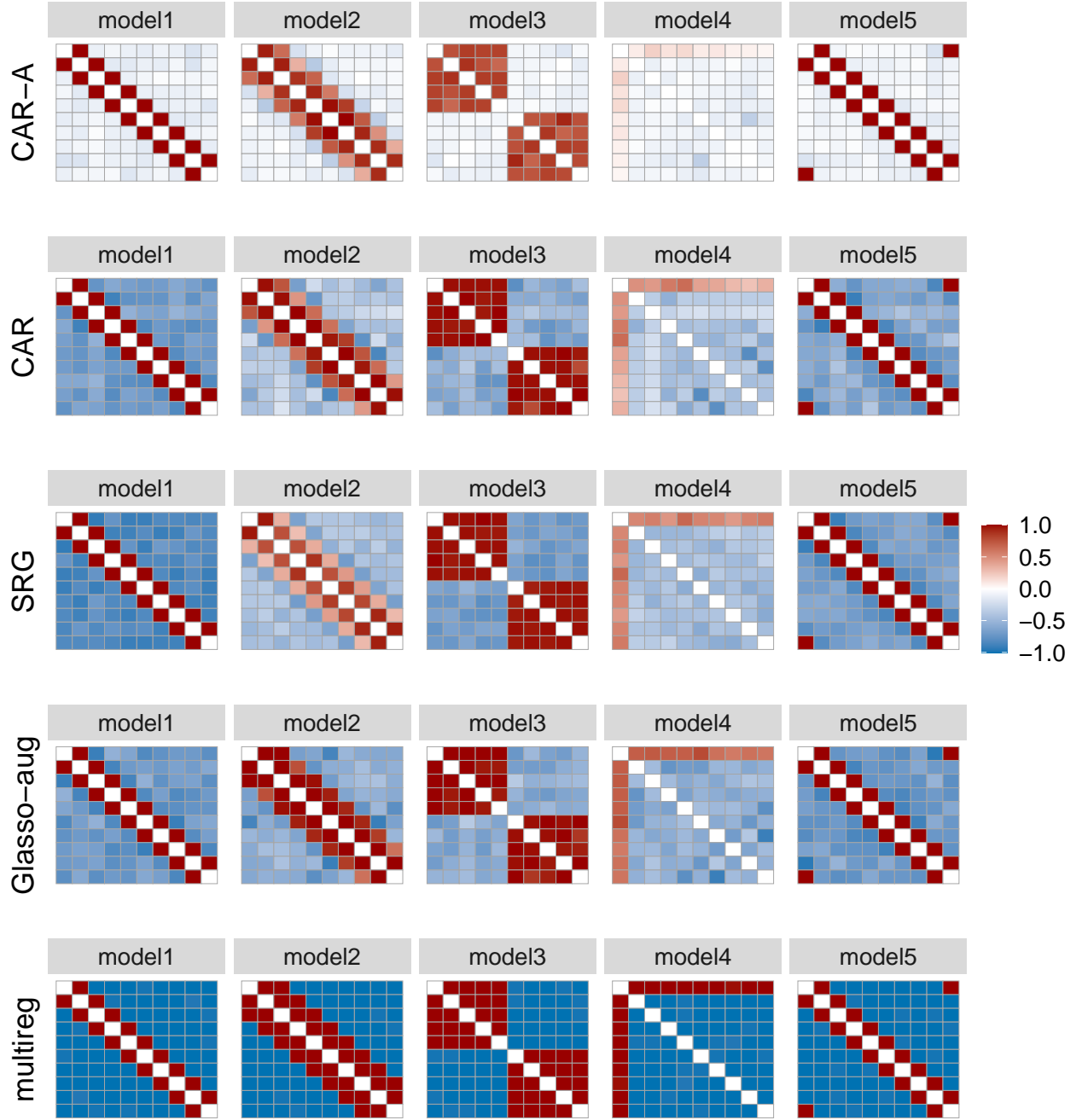


Figure A9: Reconstruction accuracy of the graph among responses (Ω) for $k = 10$ nodes, $p = 5$ predictors and sparsity of 0.8. Red entries correspond to true positive edges and blue entries correspond to false positive edges. Darker color means higher frequency of being estimated in 50 reconstructions. Our proposed method Adaptive CAR-LASSO (CAR-A) outperforms the other methods by displaying the lowest false positive rate (less blue).

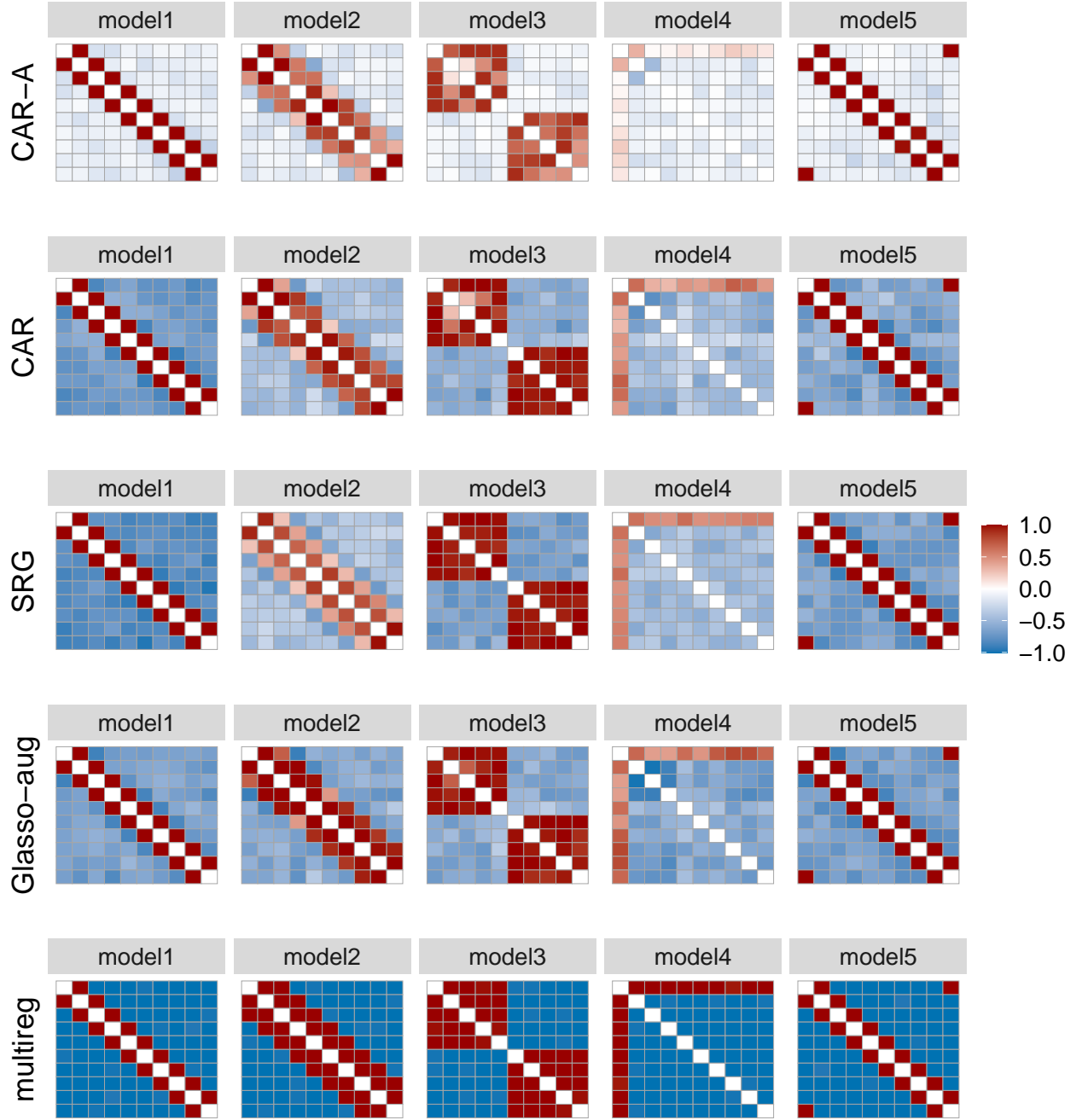


Figure A10: Reconstruction accuracy of the graph among responses (Ω) for $k = 10$ nodes, $p = 5$ predictors and sparsity of 0.5. Red entries correspond to true positive edges and blue entries correspond to false positive edges. Darker color means higher frequency of being estimated in 50 reconstructions. Our proposed method Adaptive CAR-LASSO (CAR-A) outperforms the other methods by displaying the lowest false positive rate (less blue).

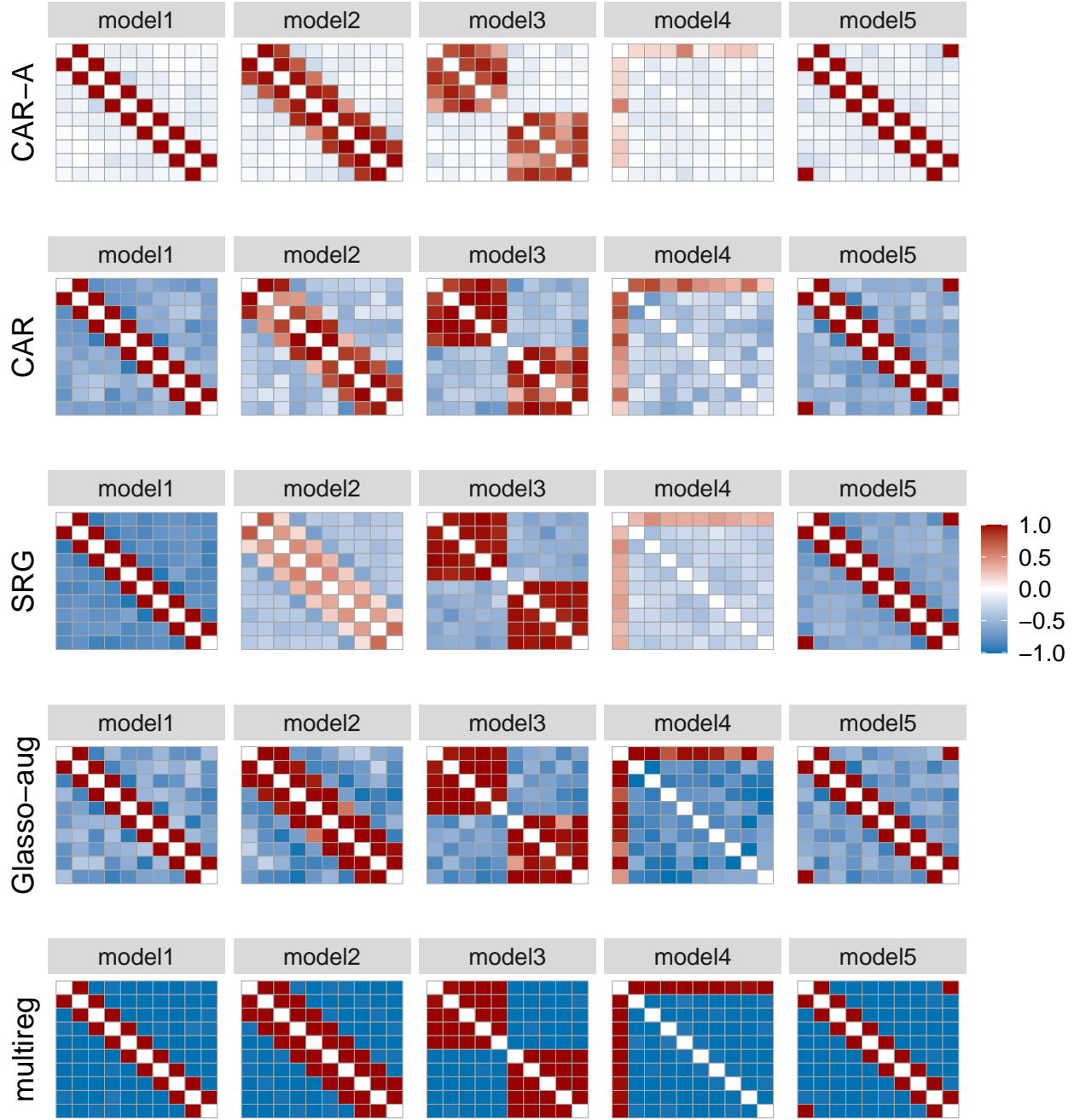


Figure A11: Reconstruction accuracy of the graph among responses (Ω) for $k = 10$ nodes, $p = 10$ predictors and sparsity of 0.5. Red entries correspond to true positive edges and blue entries correspond to false positive edges. Darker color means higher frequency of being estimated in 50 reconstructions. Our proposed method Adaptive CAR-LASSO (CAR-A) outperforms the other methods by displaying the lowest false positive rate (less blue).

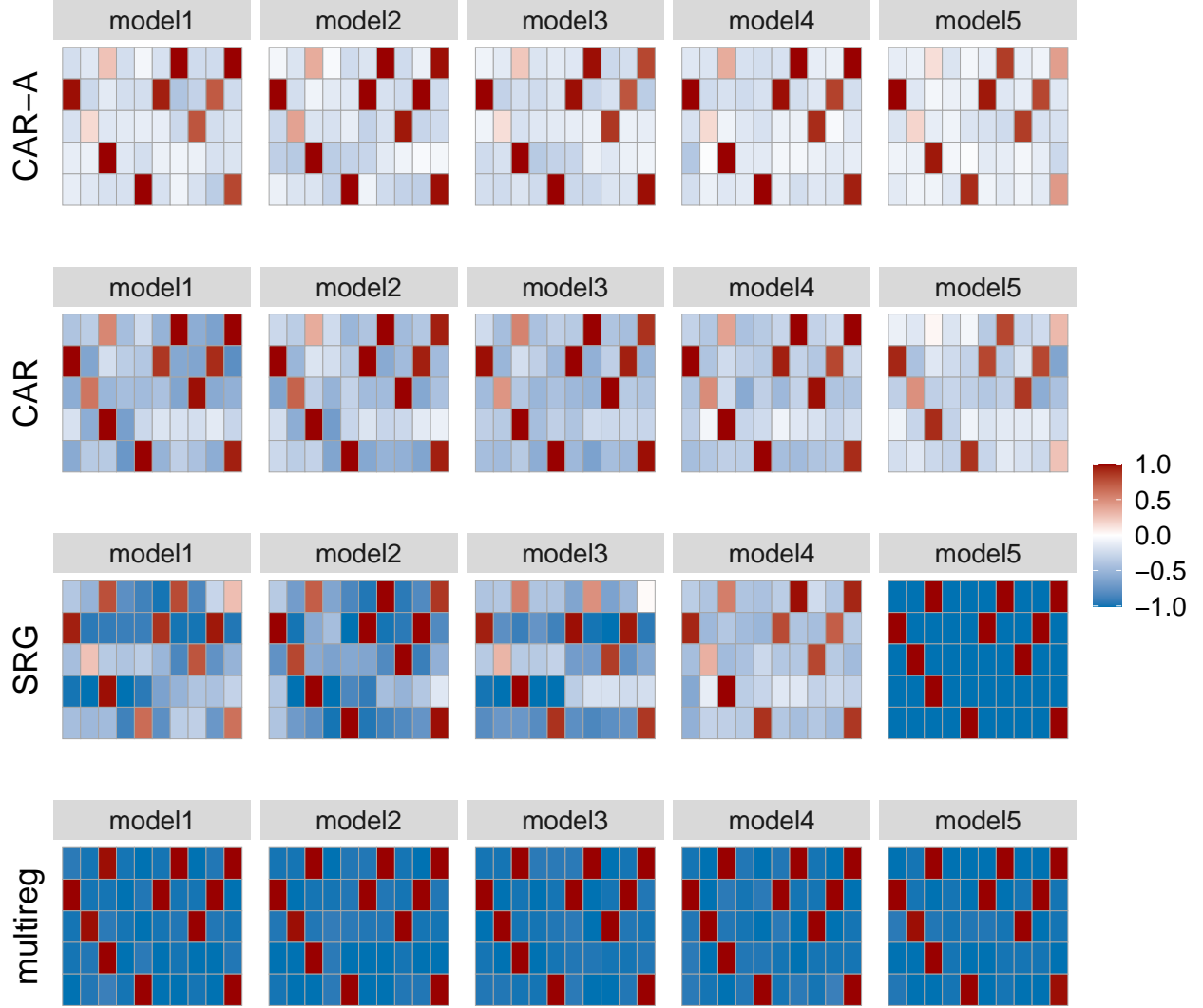


Figure A12: Reconstruction accuracy of the graph between responses and predictors (\mathbf{B}) for $k = 10$ nodes, $p = 5$ predictors and sparsity of 0.8. Red entries correspond to true positive edges and blue entries correspond to false positive edges. Darker color means higher frequency of being estimated in 50 reconstructions. Our proposed method Adaptive CAR-LASSO (CAR-A) outperforms the other methods by displaying the lowest false positive rate (less blue).

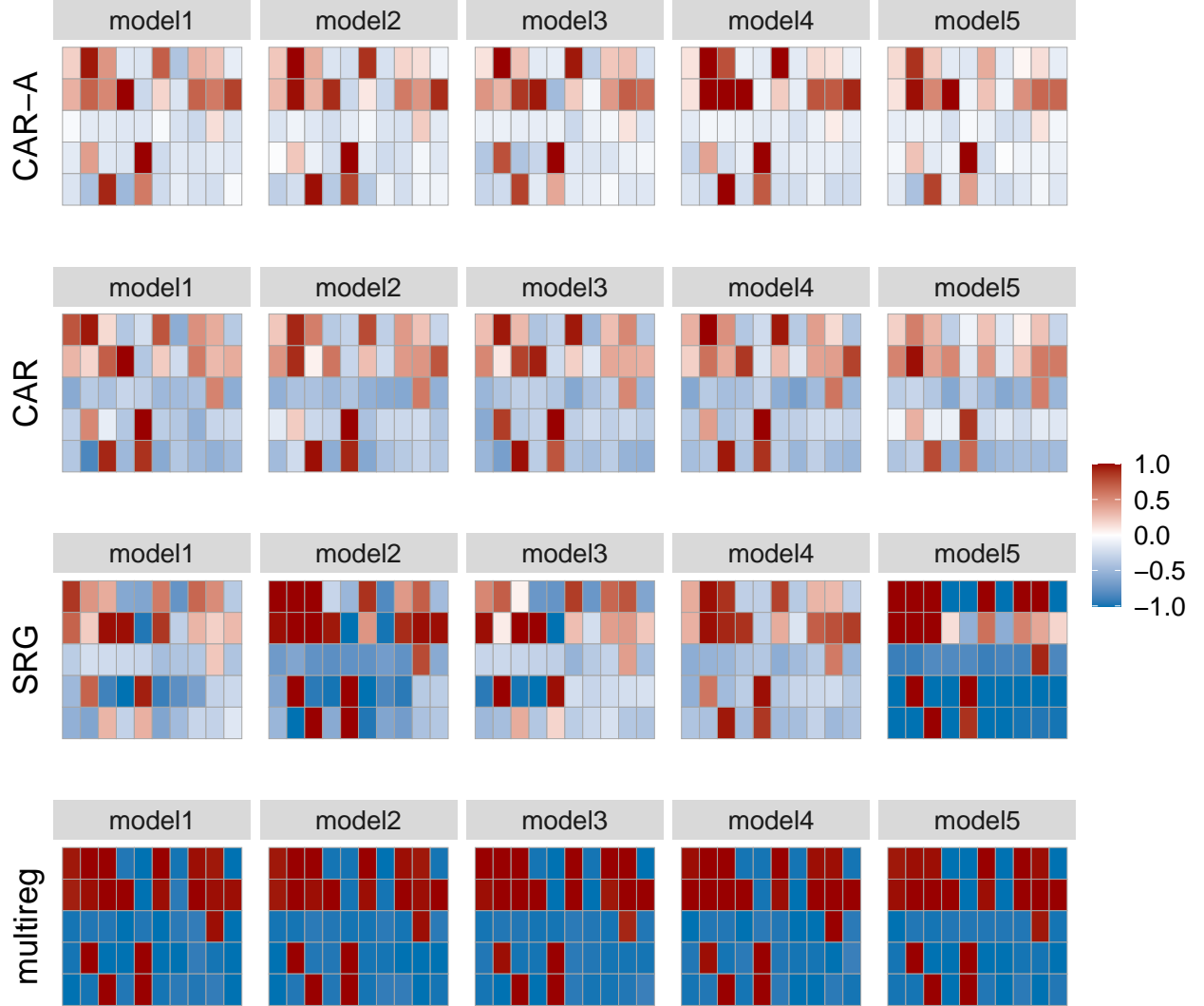


Figure A13: Reconstruction accuracy of the graph between responses and predictors (**B**) for $k = 10$ nodes, $p = 5$ predictors and sparsity of 0.5. Red entries correspond to true positive edges and blue entries correspond to false positive edges. Darker color means higher frequency of being estimated in 50 reconstructions. Our proposed method Adaptive CAR-LASSO (CAR-A) outperforms the other methods by displaying the lowest false positive rate (less blue).

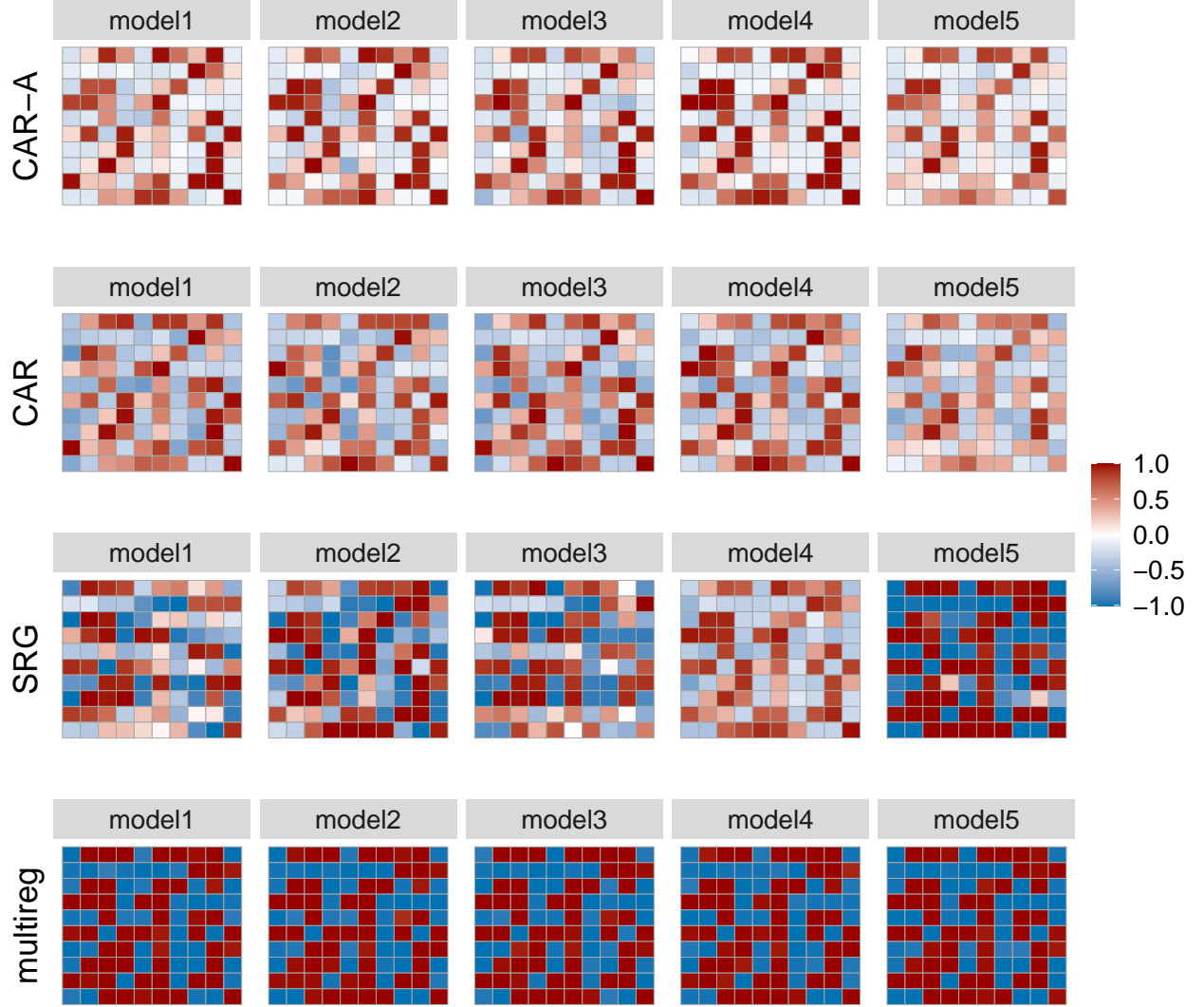


Figure A14: Reconstruction accuracy of the graph between responses and predictors (**B**) for $k = 10$ nodes, $p = 10$ predictors and sparsity of 0.5. Red entries correspond to true positive edges and blue entries correspond to false positive edges. Darker color means higher frequency of being estimated in 50 reconstructions. Our proposed method Adaptive CAR-LASSO (CAR-A) outperforms the other methods by displaying the lowest false positive rate (less blue).